

# **Ultrafast Focused High Frequency Power Doppler Imaging**

by

Bingjie Ma

A thesis submitted in partial fulfillment of the requirements for the degree of

Master of Science

In

Biomedical Engineering

Department of Electrical and Computer Engineering

University of Alberta

© Bingjie Ma, 2018

## **Abstract**

High-frequency ultrasound ( $>20\text{MHz}$ ) offers promising opportunities for high-resolution blood flow imaging of the microcirculation at superficial depths owing to high backscatter coefficient and high resolution. Because time-of-flight is minimal at these superficial depths, focused beam scanning can be done very rapidly. Ultrafast focused beam scanning is compared with traditional Doppler sequences and plane-wave imaging. Compared with traditional Doppler, ultrafast focused beam scanning is shown to offer improved sensitivity to slow flows because of higher ensemble size within an equivalent data acquisition time. Compared with plane wave imaging and plane wave compounding, ultrafast focused beam scanning is shown to exhibit lower variance and improved SNR given comparable transmit voltage levels.

# Preface

Chapter 3 discuss the research into using high frequency ultrasound focused beam to get Power Doppler images of blood flow and is primarily composed of the publications from “Ultrafast Focused High-Frequency Power Doppler Imaging”. As lead author, I was responsible for: modifying scripts of different imaging methods to satisfy experimental requirements; preparing phantoms and animals for experiments; processing the data and analyzing the results. The co-authors contributions include the following: Tarek Kaddoura helped me with simulations and experimental script modification in the early phase of my project; Min Choi helped with handling animals for in vivo experiments, especially prior to receiving my formal animal handling training; Quinn Barber helped with phantom making; Ryan Chee was the one who set up the structure of the Verasonics scripts for our high-frequency probe and for photoacoustic imaging experiments. Dr. Mrinal Mandal and Dr. Roger Zemp are my supervisors, Dr. Zemp helped to advise me with the ultrasound aspects of the project and helped modify the thesis and manuscript.

In vivo experiments involving animals described in chapters 3 in this thesis followed the laboratory animal protocol approved by the University of Alberta Animal Committee.

# Acknowledgements

A huge thank you to Dr. Roger Zemp for his support throughout my graduate work and his endless patience. His vast knowledge spanning many disciplines and his ability to balance personal and academic life are truly awe-inspiring. Thank you for your guidance throughout my research and encouraging me to continue my studies. It has been a great pleasure to work with you over the last few years.

Furthermore, thank you to another supervisor Dr. Mrinal Mandal for his patient guidance and suggestions during my graduate study. His insights were helpful, allowed this research to proceed smoothly and gave me idea on how to do scientific research.

Also, thank you to my committee members Dr. Mahdi Tavakoli Afshari and Dr. D. Joseph. Thank you for being a part of my journey through my graduate studies.

I am sincerely thankful to all my colleagues that I have worked with at the University of Alberta. Special acknowledgements to Tarek Kaddoura, Quinn Barber and Min Choi with whom I often worked closely on many different projects. The many talks during experiments we had truly stimulated my interest in research and encouraged me to continue delving the mysteries of ultrasound imaging. Thank you all for being amazing friends and colleagues.

Finally, I am profoundly indebted to my entire family who have supported me throughout my studies and encouraged me through the difficult times. Your love and support have driven me to do my very best in everything that I do. Thank you!

## Table of Contents

<b>I.</b>	<b>Introduction.....</b>	<b>1</b>
A.	Motivation.....	3
B.	Major Contributions.....	4
C.	Organization of this thesis .....	6
<b>II.</b>	<b>Background and Literature Review.....</b>	<b>8</b>
A.	Background of Ultrasound Imaging.....	8
B.	Different Ultrasound Imaging Techniques .....	12
C.	High frequency Ultrasound Imaging .....	18
1.	Flow Imaging Methods .....	19
2.	High-Frequency Blood Flow Imaging .....	20
D.	Clutter Filter.....	22
E.	Autocorrelation Color Flow Estimation Methods.....	27
F.	Vector Flow Imaging .....	29
<b>III.</b>	<b>Ultrafast Focused High-Frequency Power Doppler Imaging .....</b>	<b>34</b>
A.	INTRODUCTION .....	34
B.	Methods.....	36
1.	Experimental Setup .....	36
2.	Comparison between imaging methods .....	37
3.	Impact of UFFI Ensemble Size .....	38
4.	Testing Different Flow Velocities.....	38
5.	Filtering and Signal Processing.....	38
6.	Experiments in vivo .....	39
7.	Quality Metrics.....	39
C.	RESULTS .....	40
1.	Experiments with phantoms.....	40
2.	In vivo study.....	45
D.	DISCUSSION .....	47
E.	Conclusion .....	48
<b>IV.</b>	<b>Conclusion and Future work .....</b>	<b>49</b>

A. Summary of work done in this thesis.....	49
B. Future work.....	50
1. Clinical Translation.....	50
2. Blood velocity estimation.....	50
3. Combining Photoacoustic Imaging and Ultrafast Focused Imaging.....	50
<b>BIBLIOGRAPHY .....</b>	<b>52</b>

# List of Figures

Fig. II- 1 Reflection and refraction of a plane wave (where $c_2 > c_1$ ).....	11
Fig. II- 2 Traditional imaging method for a 4cm focal depth with $\sim 25$ fps [23] .....	13
Fig. II- 3 (a) plane-wave imaging with frame rate $\sim 18\ 000$ fps, (b) 17-angles plane-wave compounding with frame rate $\sim 1000$ fps, and (c) 40-angles plane-wave compounding with frame rate $\sim 350$ fps. [23].....	15
Fig. II- 4 PSF for different imaging methods (a) Traditional Doppler, (b) Plane Wave Imaging, and (c) Plane Wave Compound with 9 angles. (d) A transverse cut of the PSF for different methods [36] .....	16
Fig. II- 5 Contrast for different imaging methods. [36].....	17
Fig. II- 6 Ultrafast plane wave compounding for mouse’s brain. [40] .....	17
Fig. II- 7 Color doppler images with scaled color-coded velocities and directions [41].....	19
Fig. II- 8 Blood flow images at different velocities: (a) 7.4 cm/s, (b) 14.8 cm/s, (c) 22.3 cm/s, (d) 29.7 cm/s, (e) 37.1 cm/s, (f) 44.5 cm/s, (g) 51.9 cm/s, (h) 59.3 cm/s [27]. .....	21
Fig. II- 9 Overview of traditional ultrasound system [47].....	23
Fig. II- 10 Singular value decomposition (SVD)-based algorithm [53]......	25
Fig. II- 11 Data acquisition process. Each line is generating an $M \times 1$ vector. $N$ echo vectors are recorded at each line of site. Repeating the acquisition process for $L$ lateral lines of site. Recording $K$ super frames in the 4-D array of IQ data [58]. .....	26
Fig. II- 12 Power Doppler images by using HOSVD filter to show perfusion. Left column shows images of ischemic hindlimb and right column are the images of normal hindlimbs. [58]. .....	27
Fig. II- 13 Acquisition and post-treatment processing. [70]......	31
Fig. II- 14 Illustration of transverse oscillating. The apodization applied on the linear array transducer for generating left and right two beams [73]......	32
Fig. II- 15 . Transverse Oscillating vector flow image from the carotid artery. The arrows show the velocity direction, and the color shows different magnitude [61] .....	33
Fig. III-1 Data acquisition procedure of ultrafast high frequency focused imaging method. Each subset of transducer elements used to generate one focused ultrasound beam and using receive signal to create one A-scan until get whole B-scan frame.....	35
Fig. III-2 Power Doppler images of flow phantom with vessel located at 10-11mm penetration. Flow velocity is 1mm/s. (A). Plane Wave Imaging method with prf and frame rate 1KHz; (B). Traditional Doppler method with prf 1KHz; (C). 32 angles ultrafast compounding imaging method with prf 1KHz; (D). UFFI (Fast Walking Aperture) method with 32 A-scan lines for one B-scan, prf is 1KHz.....	41
Fig. III-3 Power Doppler imaes of flow phantom with two vessels located at depth of 10mm and 13mm. (A). UFFI with ensemble size 50; (B). UFFI with ensemble size 80; (C). UFFI with ensemble size 100. ....	43
Fig. III-4 Power Doppler images of flow phantom with the vessel located at depth of 8mm. The left column is imaging blood flow of 1mm/s, the right column is for 1cm/s blood flow. We use 1KHz PRF for all cases. (A) and (B). PWI method; (C) and (D). TD method; (E) and (F). 32-angle-Plane-wave compounding method; (G) and (H). UFFI method. ....	44

Fig. III-5 Power Doppler images of blood flow in the kidney of a mouse. (A). UFFI method; (B). Traditional Doppler imaging. (C) Single angle plane wave imaging. .... 46

Fig. III-6 Power Doppler blood flow images of the palm of hand. (A). PW imaging with one direction. (B) 9 angles PW imaging. (C) Traditional Doppler method. (D) UFFI (fast walking aperture) imaging method..... 47

# List of Tables

TABLE 1.....	37
TABLE 2 MEASURED SNR AND VARIANCE.....	45

## **I. Introduction**

This thesis concerns the development of new ultrafast high-frequency flow-imaging methods aimed to improve the sensitivity of detection of flow in the microvasculature. Currently, diagnostic ultrasound systems use ultrasound transducer arrays with typical frequencies of 2-15MHz. The higher the transducer frequency, the finer the spatial resolution, but the less the penetration depth. Frequencies higher than 20MHz are considered “high-frequency” in the ultrasound imaging community. While investigators have pursued research using high-frequency transducers for some time, only in the last few years have high-frequency ultrasound array transducers become commercially available. Additionally, research ultrasound platforms to accommodate these high-frequency probes have only recently been made available. This thesis aims to take advantage of these recent developments to provide new flow-imaging capabilities using high-frequency ultrasound transducer arrays for very-high resolution flow imaging with unprecedented flow sensitivity.

Ultrasound flow measurement techniques include Power Doppler and Color Doppler imaging. Color Doppler estimates flow velocities by tracking speckle motion, typically using autocorrelation-based flow estimators. This thesis focuses on high-frequency Power Doppler imaging. Power Doppler is a method which detects the scattered power of moving blood, independent of flow direction or speed. Current diagnostic Power Doppler systems have limited sensitivity to flow in microvasculature and primarily detects large vessels. High-frequency transducers offer new opportunities for imaging flow in the microcirculation given improved spatial resolution compared to diagnostic systems. Additionally, blood scattering cross-sections

are significantly larger at higher frequencies, and therefore signal from blood is much stronger than at lower diagnostic frequencies.

High-frequency Power Doppler has previously been introduced by a number of investigators [1][2][3]. Additionally, recent ultrafast ultrasound imaging methods have been shown to provide transformational improvements in sensitivity to blood flow. These new ultrafast imaging methods, unlike traditional Doppler methods acquire whole image frames at hundreds or even thousands of frames per second and track flow frame-to-frame at each pixel location. This is in contrast to more traditional methods which only track flow along lines-of-sight using a few pulsed interrogations. The larger ensemble size afforded by the ultrafast imaging methods, along with novel spatio-temporal filtering schemes, have provided stunning views of blood flows in the brain, kidneys, placenta, and other organs. However, most of these ultrafast Doppler developments have not used high-frequency transducers. Additionally, they use unfocused transmissions. For high-frequency transducers, these transducers cannot be operated at very high transmit voltages because of dangers of dielectric breakdown, among other considerations. This means that unfocused transmission methods such as plane-wave imaging methods, may not have the SNR advantages of focused imaging methods. On the other hand, current focused imaging methods for diagnostic ultrasound imaging, are relatively slow, owing to the propagation delays for each line. In contrast, given that high-frequency ultrasound is limited in penetration, time-of-flight for shallow imaging depths is minimal compared to diagnostic deep imaging methods. Because of this, high-frequency ultrasound can image using focused transmissions at fairly high frame-rates. The purpose of this thesis is to investigate whether ultrafast focused imaging methods implemented with a high-frequency array system can achieve improved Power Doppler sensitivity compared to traditional Doppler and plane-wave ultrafast imaging methods.

## A. Motivation

Work in this thesis is motivated by multiple unmet clinical needs. Potential applications for this technology may include imaging of angiogenesis (the growth of new blood vessels) in diseases such as cancer [4]. Additionally, there is an urgent unmet need for imaging perfusion in diseases such as diabetes. Diabetic complications include pressure ulcers and other sores, peripheral vascular disease etc. [5]. Currently only very crude methods exist for assessing perfusion of limbs to make difficult clinical decisions about need for amputation, etc. Early detection of deep ischemic wounds such as early-stage ulcers could enable preventative measures and save the healthcare system billions of dollars.

Early detection of cancers, including angiogenesis surrounding neoplasms, could greatly improve prognosis given the optimistic outcomes from treatment of cancers that are detected prior to metastasis [6][7].

Imaging slow blood flows and microcirculation is an challenge in imaging most organs like skin, prostate, placenta and in tumor for cancer diagnosis. Imaging tumor microcirculation is essential in diagnosis and prognosis and tracking the treatment effect of using some therapeutic agents [8]. Help on detecting blood clots in some narrow blood vessels which may increase the risk of stroke and can help monitor the flow of blood during blood vessel surgeries [9]. Several current techniques are used for visualizing blood flows of micro-vasculature. Like, Magnetic Resonance angiography (MRA) using Magnetic Resonance Imaging (MRI) [10], Computed Tomography angiography (CT-Angiography) based on Computed Tomography (CT) [11] and Positron Emission Tomography (PET) [12]. However, big challenges still coming up like poor resolution, prohibitive cost and radiation hazards. Ultrasound Imaging is a portable, lower in cost and no ionizing radiation imaging method, that has been used for imaging vasculature.

Since imaging of microvasculature is valuable for clinical and cancer studies, plus ultrasound imaging method is safe, low cost and portable, high quality ultrasound images of micro vessels is being actively investigated.

## **B. Major Contributions**

We investigate ultrafast High-Frequency focused imaging as compared with traditional Doppler, plane-wave imaging and multi-angle plane-wave compound imaging. High imaging rates are possible when imaging at superficial depths and spatio-temporal filtering approaches are possible. We use a 256-element linear array transducer with central frequency of 21MHz. We use spatiotemporal clutter filtering based on Singular-Value Decomposition (SVD) filters to remove tissue motion clutter [13]. Simulations, phantom experiments, and in vivo imaging studies are performed to compare the above-mentioned methods.

High-frequency focused beam imaging which can reach frame rates nearly as high as that of ultrafast plane wave imaging due to shallow penetration depths and minimal time-of-flight. By using larger ensemble size, high-frequency focused beam can get very good sensitivity to slow flows and have advantage of high SNR. In addition, compared Ultrafast Focused Imaging (UFFI) method (also named high-frequency fast walking aperture) with plane wave (PW) and traditional Doppler (TD) sequences.

Traditional Doppler Ultrasound sequence, the scanner transmitted 8-15 focused ultrasound beams to get a line of the image frame. UFFI also uses focused beam the same as traditional doppler. However, by transmitting one ultrasound focused wave, one reception to generate one line of the image frame, which can make this method imaging much faster than Conventional Doppler or get larger field of view within the same data acquisition time.

Plane wave imaging has the advantage of high imaging speed, which is essential to make real time imaging and diagnosis. The high frame rate of plane wave imaging as the whole image frame can be obtained through single pulse emission. But the low image quality shows as a big weakness. When imaging the shallow depth, our approach can get ultrafast imaging speed to reach almost the same speed as plane wave imaging while the image quality, such as SNR, spatiotemporal resolution, contrast etc., is much better than plane wave imaging.

Ultrafast compound imaging can improve image quality dramatically compared with flash imaging. Multi-angle plane wave imaging makes up this flaw of flash imaging to great extent, however, it still cannot get as many signals as fast walking aperture for low velocity flows ( $\sim 1\text{mm/s}$ ).

We use high-frequency ultrasound transducer (Central frequency is 21 MHz) which can get higher amount of backscatter signals [2]. However, as high frequency ultrasound will attenuate more while travel through soft tissue, we cannot image very deep since ultrasound wave intensity decrease a lot along the transmitting [8]. We combine fast walking aperture imaging method with using high frequency transducer together, we can get not only high imaging speed but also high image quality on superficial penetration depth compare with Traditional Doppler Imaging method and Plane Wave Imaging method, respectively.

For example, if we are imaging a target at depth around 7.5 mm, according to  $\lambda=v/f$ , if we use higher frequency, we will get lower wavelength. Which means we will get lower penetration. However, for animal testing (usually mouse), this penetration is enough. We want to get 7.5mm penetration, it will be 15mm length for the whole trip for both transmission and reflection.

$$15\text{mm}/(1.5\text{mm}/\mu\text{s})=10\mu\text{s}/\text{A-scan} \quad (\text{I-1})$$

Suppose we used a linear array probe with 256 elements:

$$256 \times 10 = 2560 \mu\text{s} \text{ (time for scan one image)} \quad (\text{I-2})$$

$$1/2560 \mu\text{s} = 390 \text{ frames/s} \quad (\text{I-3})$$

$$\lambda = \frac{c}{f} = \frac{1540 \text{ m/s}}{20 \text{ MHz}} = 77 \mu\text{m} \quad (\text{I-4})$$

So, we can get the axial resolution, usually equals to two times of wavelength, is 0.144mm. From the equation, we can get when using higher frequency wave, we can get better axial resolution to get better discrimination capacity.

For the blood flow imaging, main artifacts originate from surrounding moving tissue. The received echoes of tissue and backscattered blood echoes have similar characteristics, especially for slow blood flows in small-size vessels. When imaging low velocity flows of microcirculation, clutter signals from reflective slow tissue motion need to be discriminated from blood motion. Traditional Doppler use high pass wall filter to remove tissue or vessel wall motion signals and keep high frequency blood signals. Nevertheless, wall filter performs unsatisfactory for microcirculations since the velocity of blood flow and tissue motion do not have very significant difference. In this scenario, a spatiotemporal clutter filter, Singular-Value Decomposition (SVD) filter is applied to remove tissue motion clutter of ultrasound data obtained [14]. Conventional Doppler imaging can only generate very limited number of temporal frames for one spatial position, SVD filter face difficulties to get optimized microcirculation image using the low ensemble size. UFFI can make contribution to overcome this limitation by imaging at ultrafast speed to increase the ensemble size.

### C. Organization of this thesis

The rest of the thesis is organized as follows: Chapter 2 provides literature review on the state-of-art of Ultrasound blood flow imaging techniques. The work I have done presented in this thesis will be described in Chapter 3. The Chapter 3 focuses on using power Doppler method to do high frequency focused ultrasound blood flow imaging and compare with other imaging methods to show advantages. Chapter 4 summarizes the work I have done, discusses conclusions and future work direction.

## **II. Background and Literature Review**

Imaging in the medical field is over one hundred years old. Before imaging methods were available, structures inside the body could only be seen through incision. With the rapid development of technology, today imaging methods play an essential role in medicine. The main medical imaging methods include X-ray projection imaging [15], Ultrasound imaging (US), X-ray Computed Tomography (CT) [16], Magnetic Resonance Imaging (MRI) [17], Single Photon Emission CT (SPECT) [18], Positron Emission Tomography (PET) [19]. The focus of this thesis is on ultrasound imaging, and in particular, high-frequency Power Doppler ultrasound imaging.

### **A. Background of Ultrasound Imaging**

The frequency range of audible sound is from 20 Hz to 20 kHz. A longitudinal, mechanical wave over this frequency (frequency >20kHz) is called ultrasound. It is a pressure wave or displacement and must have a medium to travel through. Since Pierre Curie first discovered piezoelectric energy in 1880, it opened a door for ultrasound development [20]. The first use and development for ultrasound was the First World War in detection of submarines [21]. The first ultrasound scanner was developed in 1947 by putting patient into a water tank [22]. There are many other impressive developments of ultrasound imaging in the past decades. From real time imaging by the development of microprocessor to Doppler imaging by applying digital signal processing, then the plane wave compound and harmonic imaging and 3D even 4D imaging come to the public to now by using the GPU to process data to get ultrafast imaging [23]. Now it has become the most widely and commonly used imaging modality over the world due to no radiation

hazards, low cost, and real time imaging capabilities. However, it has several drawbacks: lack of penetration depth through bone or air cavities because of the acoustic impedance, noise from the device and human body, speckle noise confounding structure visibility, and reverberation and tissue motion artifacts [24].

Ultrasound is generated by an ultrasound transducer. There are several kinds of transducers, including linear array transducers, phased-array transducers, convex transducers etc. They will be used for the examination of different body parts according to their different properties. Linear array transducers will usually be used for imaging superficial structures, vascular system abnormalities [25].

Ultrasound transducers are used to transmit ultrasonic pulses and receive echoes. Within the transducer, there are several piezoelectric crystal elements. When a transient voltage is applied to a piezoelectric element, it vibrates at its resonant frequency (relevant to the width of the crystal) and generates an ultrasound pulse. Likewise, when a piezoelectric crystal receives the returning echo sound waves, this element produces an output electrical voltage. The piezoelectric crystals typically will have a width of one wavelength or a half-wavelength to enable minimal grating lobe artifacts during transmit and receive focusing. Signals are detected by measuring the receive voltage on a subset of elements, and then performing beamforming operations. All the backscattered echoes from one transmitted pulse are collected before transmitting the next pulse. The time-of-flight is proportional to depth and the strength of the echoes encoded scattering differences in the object associated with density and other variation. The emitted pulse is always kept very short by damping it [26].

The speed of ultrasound is determined by the properties of the travel-through medium, mainly determined by the density and elasticity of the medium. The denser the medium is, the slower

speed the ultrasound has; the more elastic the material is, the higher the speed of the ultrasound wave. The speed of ultrasound in most soft tissues of human body is around 1540m/s. Ultrasound can get the depth information by measuring the time between the emission of an ultrasound pulse and the reception of the backscattered echo. The distance can then be calculated by multiplying the speed of ultrasound and the measured time interval [27].

Ultrasound imaging technique is mainly based on measuring the echoes received back from medium when transmitting an ultrasound signal to it. In ultrasound imaging technique, the ultrasound wave interacts with targets and surrounding tissue, and some of the emitted energy returns to the transducer will be collected. The device calculates the distance between the transducer and the target using the speed of sound in soft tissue and the time measured for each echo from emission to return-back. The portion of the incident ultrasound beam which reflected from tissue interface depends on the acoustic impedances. Acoustic impedance concept is important in describing wave passing through the boundaries between medium with different properties like the density and the bulk modulus for elasticity. Specific acoustic impedance is defined by:

$$Z(r, \omega) = \frac{p(r, \omega)}{v(r, \omega)} \quad (\text{II-5})$$

where  $\omega$  is angular frequency at a spatial location  $r$ , where  $Z$  is the acoustic impedance,  $p$  is the pressure and  $v$  is the particle velocity. To represent the situation when a plane wave travel through an inviscid fluid, we can obtain:

$$Z = Z_0 = \rho_0 c_0 \quad (\text{II-6})$$

where  $Z_0$  is the acoustic impedance of the medium,  $\rho_0$  is the density of the medium, and  $c_0$  is the velocity.

When ultrasound pass through human body, plane harmonic travels through boundary between two different mediums with different properties, reflection and refraction will occur at the interface as shown in Fig. II-1:

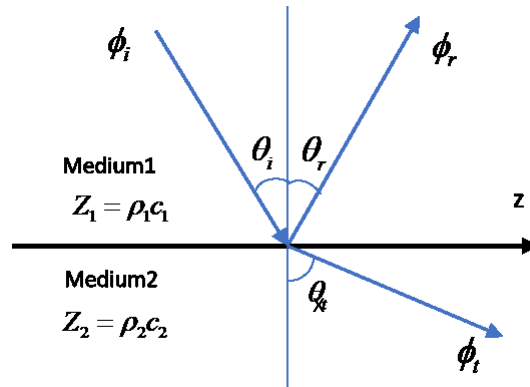


Fig. II- 1 Reflection and refraction of a plane wave (where  $c_2 > c_1$ )

According to Snell’s Law, we can obtain:

$$\frac{\sin \theta_i}{\sin \theta_t} = \frac{c_1}{c_2} \tag{II-7}$$

which describes refraction of plane-ultrasound waves at a planar interface with different sound-speeds.

When ultrasound wave passes through a medium, attenuation occurs due to absorption and re-direction of some energy by scattering because of non-uniformities in compressibility and density. The absorption appears as heat lost to surroundings from the focussed ultrasound pulse on moving molecules. Due to the differences in density, compressibility, and elasticity of different tissues

within human body, the ultrasound wave will be scattered in all directions. If the incident intensity at  $x=0$  is  $I(0)$ , the intensity at location  $x$  can be found like below:

$$I(x) = I(0)e^{-2\alpha x} \quad (\text{II-8})$$

where  $\alpha$  is the amplitude attenuation coefficient, note that the attenuation coefficient is frequency, temperature and pressure dependent. Ultrasound cannot pass through air and will be reflected completely. Bone is also highly attenuating for ultrasound due to its high intensity.

The backscattered signals will be received on the transducer and display. Especially when the ultrasound beam and different boundary are not perpendicular to each other, the ultrasound beam will be bounced off to other direction without reaching to transducer, scattering now play a significant role to make the extent of different tissue still show on screen. From this aspect, scattering is not an artifact but what makes ultrasound imaging useful for doctors to diagnose [20].

The medical machine displays the distance and intensity of the received signal on the screen. Superficial-depth structures such as skin, tendons, breast and the brain are imaged using high frequencies, which can provide better spatial resolution at the cost of penetration. Deeper structures like liver and kidney will be imaged using lower frequency with lower spatial resolution but with better penetration [28].

## **B. Different Ultrasound Imaging Techniques**

Most traditional ultrasound systems send focused pulses and receive and beamform the echoes one line at a time. This method is frame-rate limited by the time-of-flight of ultrasound and the number of scanlines acquired (sometimes called A-scans) within a 2D B-scan.

Conventional ultrasound imaging sequentially transmits focused ultrasound beams to different lines, and for each transmit event beamforms the reflected backscattered echoes from transducer

elements to generate one A-scan line of a 2D B-scan image (See Fig.II-2). The maximum frame rate to generate such a focused beam image can be calculated as:

$$FR_{focused} = \frac{c}{2d} \cdot \frac{1}{n\_lines} \quad (II-9)$$

where  $c$  is the speed of ultrasound within soft tissues in human body,  $d$  is the distance from ultrasound transducer,  $n\_lines$  is the number of lines for one whole frame. We can see the frame rate is strongly depending on the depth of penetration and the number of lines for one B-scan frame.

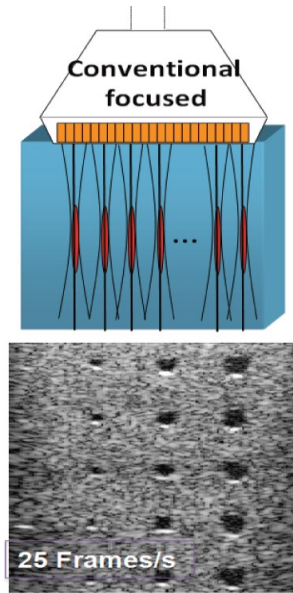


Fig. II- 2 Traditional imaging method for a 4cm focal depth with ~25fps. Reproduced with permission from [23]

Recently, fast imaging methods have been developed including fast synthetic aperture imaging [29], diverging wave imaging [30], and plane-wave imaging methods [31]. These ultrafast methods are providing transformational flow imaging capabilities [24] as well as enable methods such as shear-wave elastography and acoustic radiation force impulse imaging [32]. This thesis focuses on

the development of ultrafast focused beam imaging methods and comparing with plane-wave imaging methods with a focus on high-frequency Power Doppler imaging.

Plane wave imaging, as the name suggests, uses unfocused plane-wave transmissions. The use of ultrasound plane wave or diverging waves has been studied for several years. This technology enables attainment of ultrafast imaging to get frame rates higher than 1000 frames per second. Modern digital signal processing units, Field Programmable Gate Arrays (FPGAs) [23] and Graphical Processing Units (GPUs) are playing a vital role in fast processing for real-time realization of next-generation ultrafast ultrasound imaging platforms [33].

For single plane-wave transmission imaging, the image quality obtained is low, owing to lack of transmit focusing, but offers the advantage of high imaging speed, which is critical in emerging ultrafast flow and elastography applications [34]. An approach to improve the one angle plane wave imaging is to transmit several tilted ultrasound beams towards different angles, these ultrasound waves are sent to the target location and the backscattered signals will be combined together to produce a full image [35]. This angle compounding strategy significantly improves image quality compared to single-plane-wave imaging while still maintaining high image quality [32]. Such strategies have enabled high quality blood flow imaging (See Fig. II-3 (a), (b) and (c)) [36].

Plane wave imaging needs to compromise among contrast, resolution and sensitivity which is important when imaging weak and slow blood flow scatterers. The main limitation of conventional Doppler modes is we cannot detect and image blood flows in very small vessels (capillary with diameter 50-200 $\mu\text{m}$ ) and with very low sensitivity.

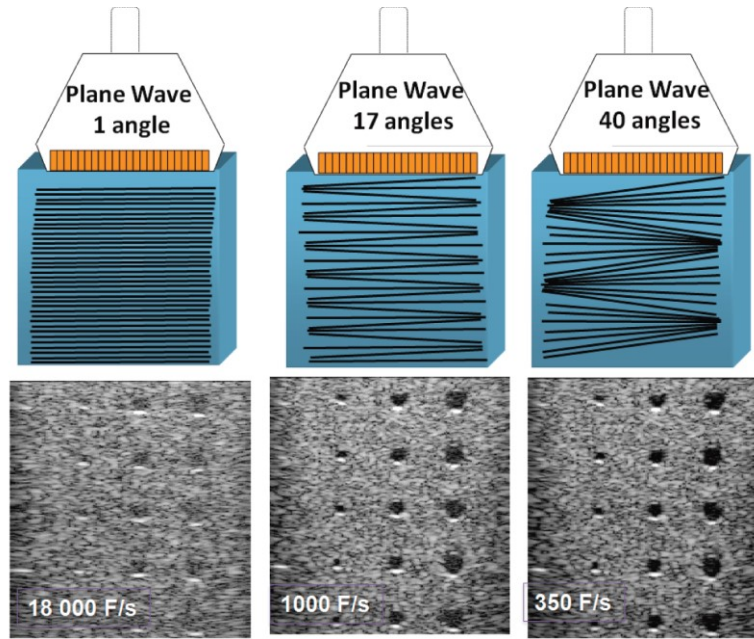


Fig. II- 3 (a) plane-wave imaging with frame rate  $\sim 18\,000$  fps, (b) 17-angles plane-wave compounding with frame rate  $\sim 1000$  fps, and (c) 40-angles plane-wave compounding with frame rate  $\sim 350$  fps.

Reproduced with permission from [23]

To illustrate the trade-offs in imaging speed, resolution, and image quality, consider the point-spread-function (PSF) study by [37]. A PSF is the image formed from a point target. The degree of blurring of this point target is a frequently used and useful measurement of the quality of the imaging system [38]. Fig.II-4 is a PSF acquired using a linear array transducer with 128 elements, with pitch of 0.3mm and central frequency of 5MHz. The voltage used for the transducer is 50V. The maximum angle used for ultrafast compound approach is  $9^\circ$  and the sampling frequency is 20 MHz. A wire with  $50\mu\text{m}$  radius in water is used for comparing different approaches.

Fig. 4 shows the PSFs acquired with different imaging methods. The point is located at a distance 8mm from transducer. The ultrafast compound plane wave imaging method can achieve very good quality PSF without much blurring (See Fig. II-4).

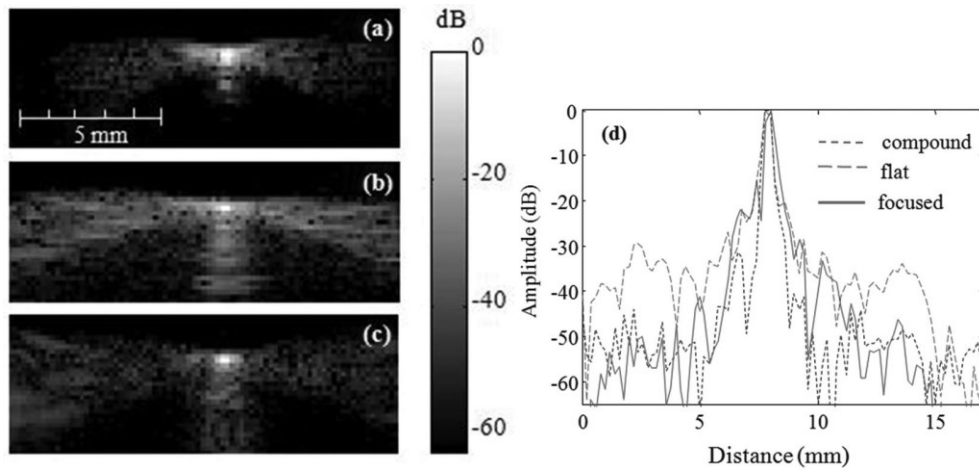


Fig. II- 4 Point-Spread Functions (PSFs) for different imaging methods (a) Traditional Doppler, (b) Plane Wave Imaging, and (c) Plane Wave Compound with 9 angles. (d) A transverse cut of the PSF for different methods. Reproduced with permission from [36]

Researchers have done several experiments and show that when using the number of angles larger than 40, the image quality, e.g., image contrast, SNR (signal to noise ratio) and resolution, will reach that of conventional focused beam method [32]. Because of the increase of number of angles, the data acquisition time is increased by a factor of 3-6, which depends on the number of lines defined for conventional focused imaging. The more angles used for ultrafast compound imaging, the better image quality we can achieve [39]. Fig. II-5 shows the image contrast as a function of increasing number of plane-wave transmit angles.

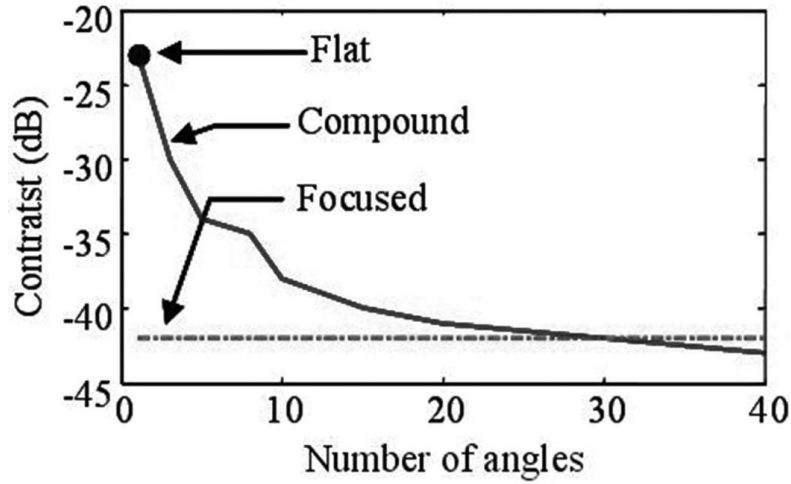


Fig. II- 5 Contrast for different imaging methods. Reproduced with permission from [36]

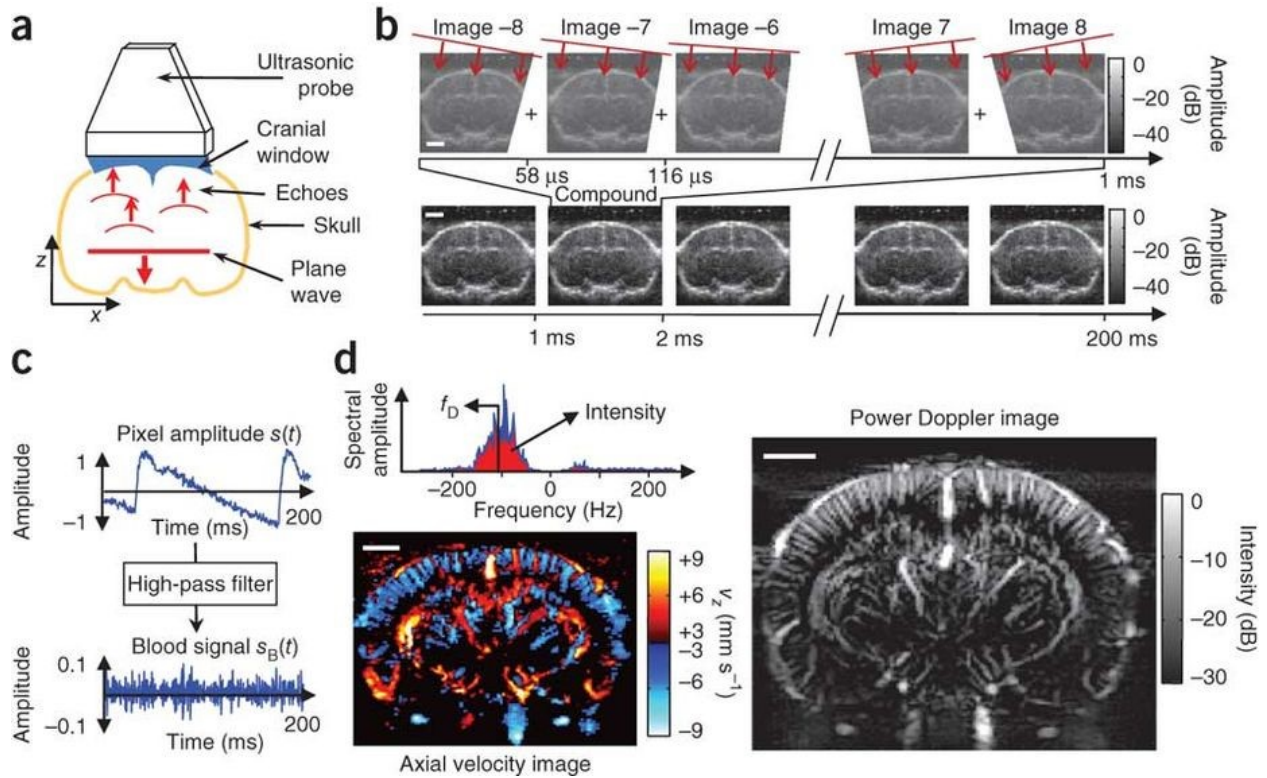


Fig. II- 6 Ultrafast plane wave compounding for mouse's brain. (a) Schematic of the imaging geometry. (b) Illustration of the plane-wave compounding imaging scheme and pulse sequence. (c) illustration of the

processing to extract blood flow (d) ultrafast color Doppler image of blood flow in the brain (bottom center) and Power Doppler image of the same (bottom right). Reproduced with permission from [40]

Recently, ultrafast plane-wave compounding methods have gained considerable attention in the literature for applications including functional brain imaging [40] (Fig. II-6), and other applications .

### C. High frequency Ultrasound Imaging

High frequency ultrasound usually refers to center frequencies above 20MHz. Most diagnostic clinical systems use frequencies in the 1-15MHz range, and most high-frequency ultrasound work has focused on pre-clinical applications. However, recently ultrasound systems have emerged in the commercial market for high-frequency clinical imaging including prostate imaging, pediatric imaging, and small-parts imaging (e.g. Exact Imaging, FUJIFILM Visualsonics Inc.). With higher frequency, improved lateral and axial resolution can be offered. The primary drawback of high frequency ultrasound wave is that it has higher attenuation than diagnostic frequencies. The attenuation can be described as below:

$$I = I_0 e^{-2\alpha x} \quad (\text{II-10})$$

where  $I_0$  is the initial intensity,  $I$  represent the intensity after ultrasound wave passing along the distance  $x$ ,  $\alpha$  is the attenuation coefficient and is proportional to frequency [14]. When the penetration depth goes deeper, high frequency ultrasound waves will be strongly attenuated. Typical penetrations of 20MHz ultrasound are  $\sim 1$ cm, compared with multiple centimeters for diagnostic ultrasound.

## 1. Flow Imaging Methods

Doppler imaging estimates vascular flow by tracking blood echoes. While continuous and pulsed-wave Doppler systems measure blood motion along a single line-of sight, Color and Power Doppler methods provide images of flow through a large field of view.

Color Doppler ultrasound measures blood flow shifts between successive interrogations to form estimates of blood flow velocity along the beam direction. Speed and direction are displayed. Typically, red color expresses a positive shift showing blood cells approaching the transducer, while blue color shows negative one for cells moving away from the transducer.

### a) *Color Flow Imaging*

In Color Flow Imaging, also called Color Doppler Imaging, we can estimate the velocity and direction of flows. The velocity may be estimated from the phase shift of ultrasound backscattered echoes. The blood velocity is estimated along every scan lines and form an image of flow. Then we combine the flow pattern with the B-mode image, and the velocity is coded as the intensity of color and direction is coded as assorted color (See Fig. II-7 as an example).

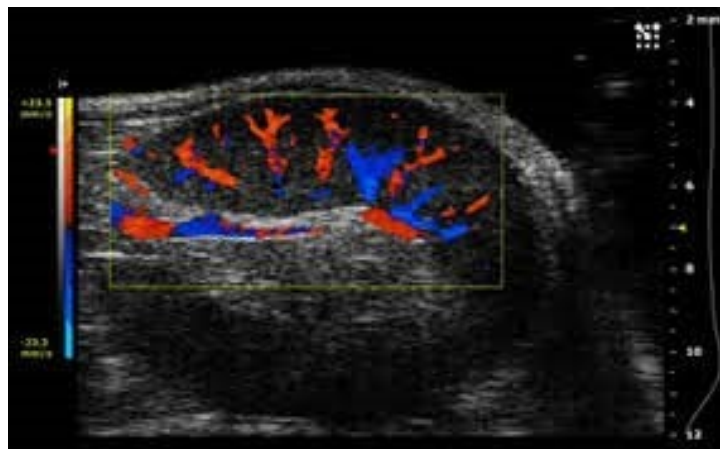


Fig. II- 7 Color doppler images with scaled color-coded velocities and directions. Reproduced with permission from [41]

For the normal B-mode image, only the amplitude of the backscattered echoes is imaged. For blood flow visualization, the phase shift or frequency change can be detected as well as the amplitude. This technique is the autocorrelation method of blood flow velocity estimation introduced by Kasai in 1985 [41][42].

### ***b) Power Doppler***

Power Doppler displays the power of moving scatterers independent of speed and direction. It has greater sensitivity to detect vasculature compared to color Doppler in part because of insensitivity to the Doppler angle between the blood flow and ultrasound beam. However, no velocity and flow direction information can be provided [43]. This benefit helps in imaging vessels with very low velocity flow, a limitation of color Doppler.

This thesis focuses on improved Power Doppler methods at high-frequencies. However, our ongoing work is aiming to use similar methods to also improve Color Doppler. Hence flow estimation methods will also be reviewed here. First, we introduce Clutter filters as they are common to both Power and Color Doppler methods.

## **2. High-Frequency Blood Flow Imaging**

Improved imaging of blood flow at high frequencies is the main focus of this thesis. Previously many groups have reported progressively improved efforts to image blood flow at frequencies over 20 MHz. Ferrara [1] reported using transducers with a central frequency of 38 MHz to detect flow in vessels with diameter as small as 40 $\mu$ m. And Vogt and Ermert [3] used 50MHz central frequency transducers to image flow phantoms with inner diameter 500 $\mu$ m. Christopher implemented an

experiment with 50MHz frequency transducer measured the blood flow in human veins with 250 $\mu$ m diameter [44].

The major difficulties of current Doppler imaging is detecting and imaging small vessels with sufficient spatial resolution and extract blood signals from moving tissues with acceptable signal-to-noise ratio [41].

High frequency ultrasound can be used for monitoring the anti-vascular effect of blood flows in tumors. With the major limitation (shallower penetration depth) of using high frequency ultrasound, high frequency ultrasound imaging will be determined largely by the tissue properties and tissue motion in the ROI (region of interest). Therefore, high frequency ultrasound offers promising opportunities for high-resolution blood flow imaging at superficial depths. Unlike traditional imaging, using high frequencies can maintain most information for the image.

One blood flow imaging method mentioned by Yang [27] (see fig.II-8) involves, sampling multiple times in the same ROI, then subtracting two adjacent temporally images to cancel out the image of tissue, thus leaving only the blood flow image.

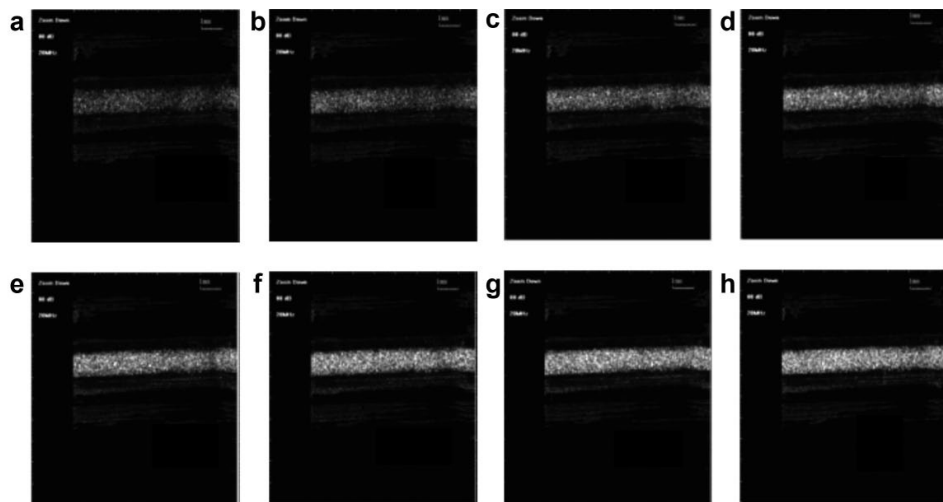


Fig. II- 8 Blood flow images at different velocities: (a) 7.4 cm/s, (b) 14.8 cm/s, (c) 22.3 cm/s, (d) 29.7 cm/s, (e) 37.1 cm/s, (f) 44.5 cm/s, (g) 51.9 cm/s, (h) 59.3 cm/s. Reproduced with permission from [27].

The system uses a 20-MHz single-element ultrasonic probe with a focal length of 14 mm and aperture of 5 mm for the transducer, and the number of repetitions  $N$  is set to 4 with a 50- $\mu$ s interval. The probe is driven by a step motor, and data are collected only in one direction of its movement. There are 800 lines per frame, so the frame rate is approximately 3 frames per second (fps). The lateral dimension of the B-scan is 14.5 mm. The dynamic range of the gray scale of the images is 48 dB (8 bits).

Most of the existing high-frequency flow imaging methods track blood-flow shifts along a single line of sight using traditional Doppler processing methods. Swept-scan methods with a single-element transducer use a slight modification of this approach. Only in the last decade have high-frequency linear arrays been commercialized and only in the last few years have systems become available for researchers to implement new imaging techniques with high-frequency imaging transducers. This thesis takes advantage of these new developments. We not only improve upon traditional Doppler methods by investigating ultrafast plane-wave compounding methods for flow tracking as discussed above, but we also introduce ultrafast focused imaging methods.

#### **D. Clutter Filter**

Clutter filters, also sometimes called wall filters are filters applied to reject tissue signals and preserve signals from moving blood. For traditional ultrasound imaging (See Fig.II-9 for the imaging system setup), one method of clutter filtering is to use a high pass filter as a wall filter to remove the clutter as the clutter signals have a lower frequency compared with blood signals. After this step we may perform Power Doppler imaging to integrate signals from moving blood, or we can perform velocity estimation as described in the next section. However, it is often difficult to

discriminate slow-moving blood signals from tissue signals, especially when tissue is moving due to vessel pulsatility, breathing, or other tissue motion artifacts [14][45].

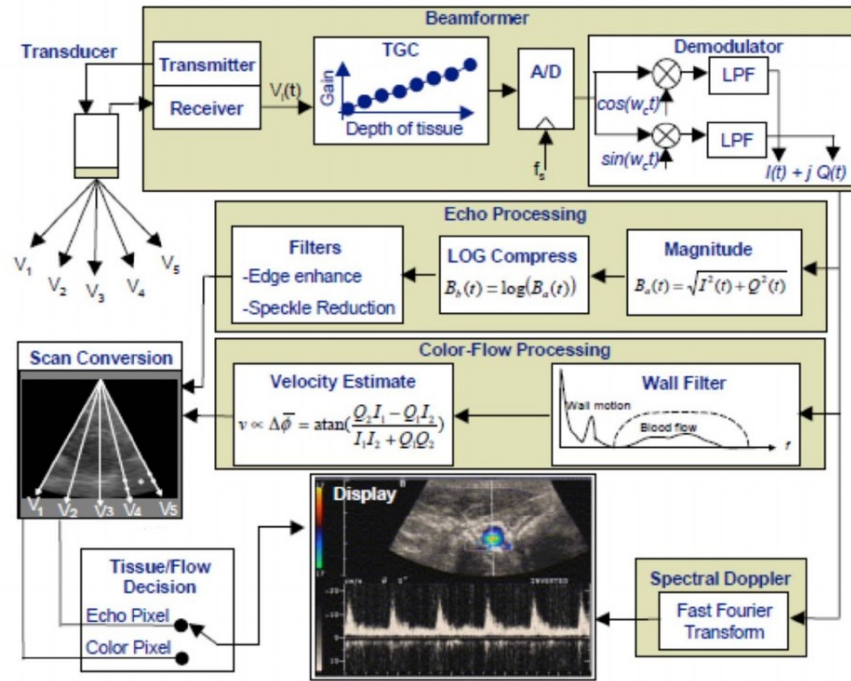


Fig. II- 9 Overview of traditional ultrasound system. Reproduced with permission from [47]

More recently, Singular Value Decomposition (SVD) filters have been applied to decompose signals into singular vectors associated with singular values rank ordered in terms of their respective power components. Filters are constructed by retaining only singular values associated with components thought to be associated with blood flow [46][47]. This successful approach has primarily been applied to tracking flow along multiple interrogations of a fixed A-scan line-of-sight. Additionally, this approach presumes signals are wide-sense stationary random processes for a Fourier Transform (Kharhunen-Loeve Transform) to enable proper filtering.

A more recent approach is the Singular Value Decomposition Filter (SVD filter), a Principal Component Analysis (PCA) based filter. This approach was first described for blood flow imaging

by Yu et al [48] for tracking flow along a single line-of-sight. It has since been generalized to ultrafast flow imaging for spatio-temporal (rather than purely temporal) filtering. The ability to track motion both temporally along a line of sign, and spatially has been used with great success in discriminating very weak flows otherwise invisible to traditional Doppler methods [49]. Since clutter signals are more coherent than the blood signals, SVD filter can be exploited to separate tissue motion and blood flow [50].

One paper regarding using a high frequency ultrasound system (Verasonics Vantage system, Redmond, WA, USA) and a high frequency linear array transducer with 256-element (MS550D, FujiFilm VisualSonics, Toronto, ON, Canada) to acquire the IQ signals. The central frequency of the transducer is 40 MHz. Seven multi-angles plane wave were transmitted for acquiring the IQ signals from different angles. A SVD-based filter was used to extract the blood signal [51]. In order to overcome the computational burden, as shown in Figure 10, sliding windows were used to extract the blood signal. Each set of three-dimension data (depth, width, time) was reshaped into a set of two-dimension data (depth×width, time) to get the covariance matrix [52].

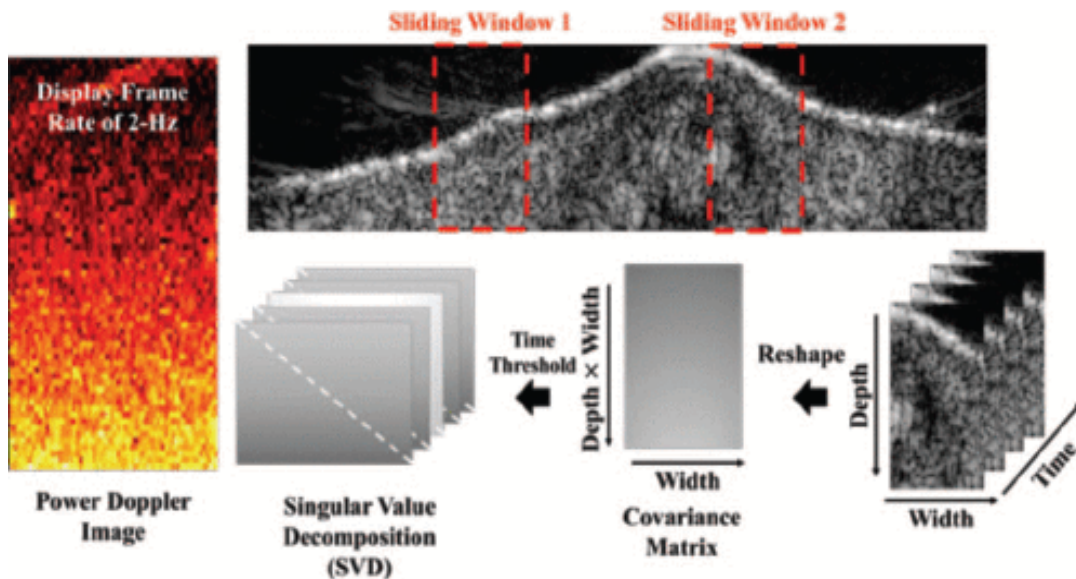


Fig. II- 10 Singular value decomposition (SVD)-based algorithm. Sliding windows are tracked over time and data is reshaped (bottom right) and a Covariance matrix is estimated (bottom, second right). This is then decomposed via singular value decomposition. Dominant singular values represent strong tissue scattering components, which are removed to leave blood signal which are then integrated to form a Power Doppler Image (left). Reproduced with permission from [53].

One very recent paper published extends the SVD filter to 4 dimensions[53], two spatial dimensions plus filtering over short ensemble sizes along single A-scans, plus filtering over multiple frames [54]. This approach enabled more effective separation of different signal components but required very long (tens of seconds) acquisition times, which may not be practical [48]. Additionally, the processing overhead is computationally burdensome given the expensive nature of the singular value decomposition [55]. The data acquisition array is showing in Fig.II- 11. One ultrasound focused pulse transmission, M temporal samples are received at fast time sample frequency. For each line, echoes are recorded N times after every N pulses emission and ultrasound beam are sent at the slow time interval which is the pulse repetition interval [56]. L lines of echo data laterally separated by the spatial interval are recorded. A packet of data array ( $N \times M \times L$ ) is called a Doppler frame. And K number of Doppler frames will be recorded in total [57].

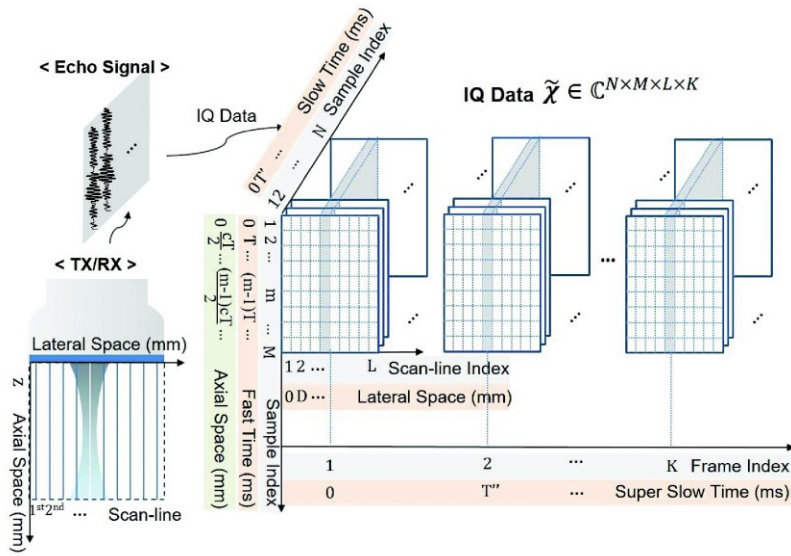


Fig. II- 11 Data acquisition process. Each line is generating an  $M \times 1$  vector.  $N$  echo vectors are recorded at each line of sight. Repeating the acquisition process for  $L$  lateral lines of sight. Recording  $K$  super frames in the 4-D array of IQ data. Reproduced with permission from [58].

Example in vivo flow data is shown in Fig.II-12. Power Doppler image of hindlimb after 3<sup>rd</sup> order SVD filtering (in this case identical to eigenfiltering) is shown below:

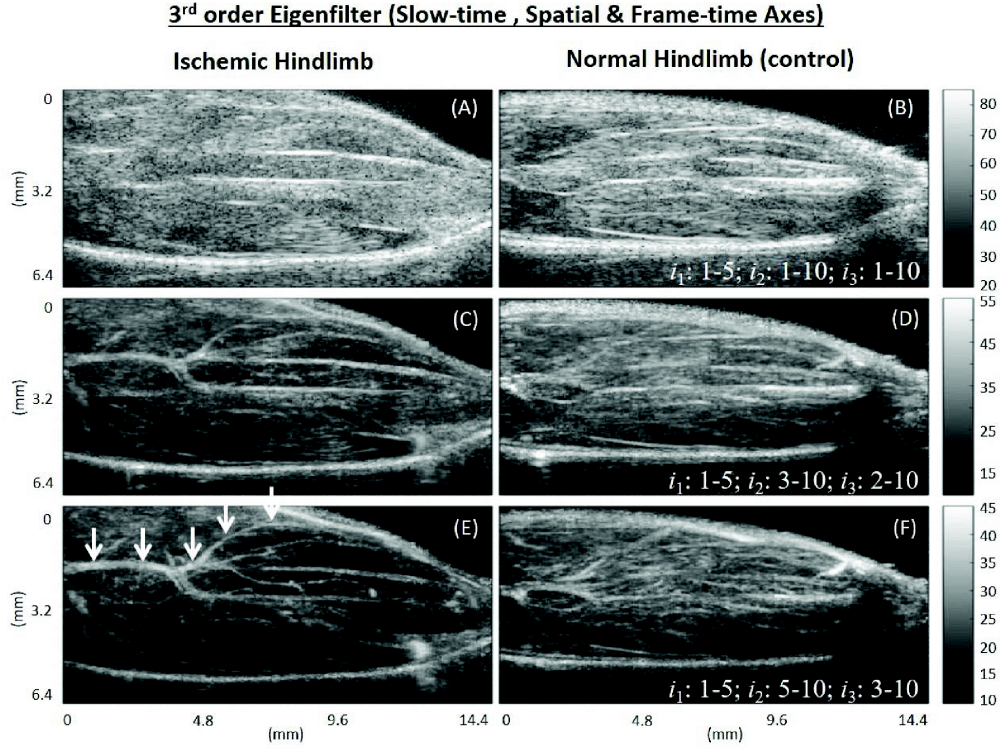


Fig. II- 12 Power Doppler images by using HOSVD filter to show perfusion. Left column shows images of ischemic hindlimb and right column are the images of normal hindlimbs. Reproduced with permission from [58].

### E. Autocorrelation Color Flow Estimation Methods

Received beamformed RF or in-phase and quadrature echo signals are used for flow estimation. The velocity of the blood can be calculated by getting the derivative of the phase of signals. The received complex signal can be expressed like below:

$$r(t) = x(t) + iy(t) \tag{II-11}$$

The phase information a signal is:

$$\Phi(t) = \arctan \frac{y(t)}{x(t)} \tag{II-12}$$

The derivative of the phase with time t is:

$$\frac{d\Phi(t)}{dt} = \frac{d \arctan \frac{y(t)}{x(t)}}{dt} = \frac{1}{1 + \left(\frac{y(t)}{x(t)}\right)^2} \times \frac{d \frac{y(t)}{x(t)}}{dt} = \frac{x(t) \dot{y}(t) - y(t) \dot{x}(t)}{x^2(t) + y^2(t)} \quad (\text{II-13})$$

$$\text{Where } \dot{y}(t) = \frac{dy(t)}{dt}, \text{ and } \dot{x}(t) = \frac{dx(t)}{dt} \quad (\text{II-14})$$

What we measured are discrete time data, when we consider y are varied slowly, we can roughly get:

$$\frac{d\Phi(t)}{dt} \approx \frac{\Delta\Phi(k)}{\Delta k} = \frac{x(k)[y(k) - y(k-1)] - y(k)[x(k) - x(k-1)]}{x^2(k) + y^2(k)} = \frac{y(k)x(k-1) - x(k)y(k-1)}{x^2(k) + y^2(k)} \quad (\text{II-15})$$

$$r(t) = ag(t)e^{-i(2\pi f_0 \frac{2v_z}{c} t)} \quad (\text{II-16})$$

Where g(t) is the envelop of the pulse.  $v_z$  is the velocity along the z direction which the direction of ultrasound beam transmission. Then we can get the equation below from equation (II-6):

$$\frac{d\Phi}{dt} = \frac{d\left(-i(2\pi f_0 \frac{2v_z}{c} t)\right)}{dt} = -2\pi \frac{2v_z}{c} f_0 \quad (\text{II-17})$$

In ultrasound imaging, we send pulses with the time difference which named pulse repetition interval,  $T_{PRF}$ . From equation (18), we use  $T_{PRF}$  to be the time difference and we can get the relation between phase shift and autocorrelation [41][58]like:

$$\begin{aligned} \Delta\Phi(T_{PRF}) &= \Phi(t + T_{PRF}) - \Phi(t) \\ &= \arctan \frac{y(t + T_{PRF})x(t) - x(t + T_{PRF})y(t)}{x(t + T_{PRF})x(t) + y(t + T_{PRF})y(t)} \\ &= \arctan \left( \frac{\text{Im}\{R(T_{PRF})\}}{\text{Re}\{R(T_{PRF})\}} \right) \end{aligned} \quad (\text{II-18})$$

where  $R(\cdot)$  is the autocorrelation function.

Combining (II-17) and (II-18) together, we can get:

$$\begin{aligned}
 v_z &= \frac{-cf_{PRF}}{4\pi f_0} \arctan \left( \frac{\text{Im}\{R(T_{PRF})\}}{\text{Re}\{R(T_{PRF})\}} \right) \\
 &= \frac{-cf_{PRF}}{4\pi f_0} \arctan \left( \frac{\frac{1}{N_c - 1} \sum_{i=0}^{N_c-2} y(k+1)x(k) - x(k+1)y(k)}{\frac{1}{N_c - 1} \sum_{i=0}^{N_c-2} x(k+1)x(k) + y(k+1)y(k)} \right) \quad (\text{II-19})
 \end{aligned}$$

Equation (II-19) is the foundation for the next velocity estimation steps. The more lines that are used for estimation, the more accuracy is expected in the estimation. In (21), the numerator and denominator are calculated according to all the samples obtained to find the phase shift. From the equation we can see the phase shift estimation relies on calculating the derivative of the received signals. An improved estimate could be achieved by using a high order difference equation [42].

The estimation is calculated from the autocorrelation. The estimation of the mean velocity can provide indication of the flow rate [59].

## F. Vector Flow Imaging

Recent vector flow imaging methods have enabled estimation of velocity and direction information at every pixel [60]. Ultrafast compound imaging using multi-angle plane wave emissions to obtain large amount frames for vector velocity estimates to generate a blood flow motion image at the frame rates in the doppler pulse repetition frequency [61]. Pixel values in the image sequence at different location and time are computed from IQ data of each pixel after the wall filter.

These sequences can capture motions with the speed same as frame rate which equals to the PRF (pulse repetition frequency). It introduces a full image of flow dynamics as a motion in the blood flow reflectivity [62]. This approach can get frame rate around 500 fps compared with 30 to 40 fps for the traditional color doppler imaging, which make it possible to provide quantification of very fast transitory within cardiac cycle which cannot be detected by conventional scan [63].

In recent years, new technique with cross-beam Doppler flow vector estimation has been implemented. The new implementation has: 1) single line, multi-gate flow vector estimation [64], and 2) vector flow mapping for the whole filed of view [65]. The multi-direction velocity estimation has been used of plane wave transmission to enhance the frame rate [66] and least-squares flow vector estimation [67], which has become clinically available as a real time diagnostic mode in Mindray's new Resona 7 platform. Another approach has combined synthetic aperture imaging, spread spectrum approach and using frequency coded waveforms in parallel to enhance the imaging speed [68].

In order to manage the real time imaging, each element processes its own emission or reception electronic board with its own 2M bytes memory which can store successive transmission and reception. Beamforming can be programmed and stored in a RAM. Backscattered RF signals are stored in 2Mbytes memory and transport into computer after acquisition, which can obtain around 300 RF datasets (~60mm depth) each sequence. The vector displacement can be measured between two plane wave frames by implementing the speckle tracking technique (1-D cross-correlation algorithm) on successive speckle images (i.e., two successive left images and two successive right images).

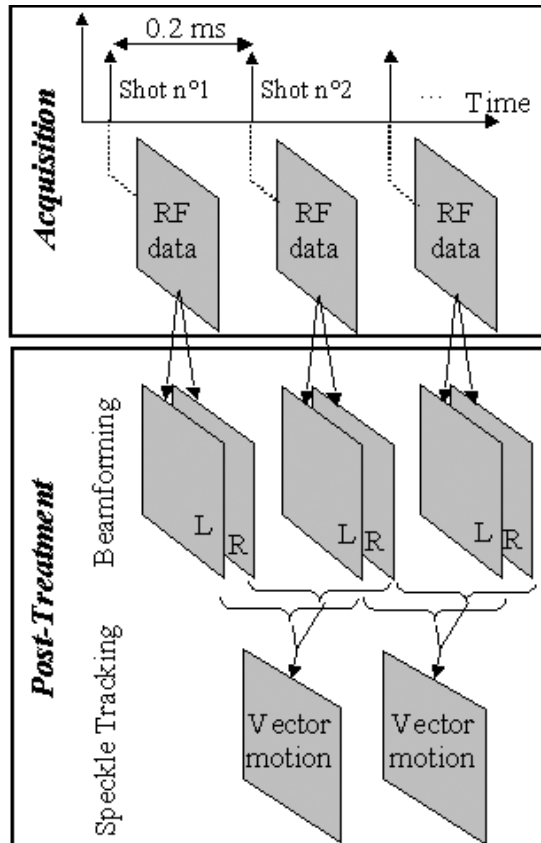


Fig. II- 13 Acquisition and post-treatment processing for typical vector flow imaging methods

Reproduced with permission from [70].

Traditional Doppler approaches can only estimate axial direction component of flow velocity to the transducer [69]. It is difficult to demonstrate complex flow patterns [70]. The Transverse Oscillation (TO) can be generated by using receiving apodization with two peaks to make a transverse oscillation [71] (see Fig II-14). A transverse movement to the ultrasound beam can yield frequency proportional to the transverse velocity [72].

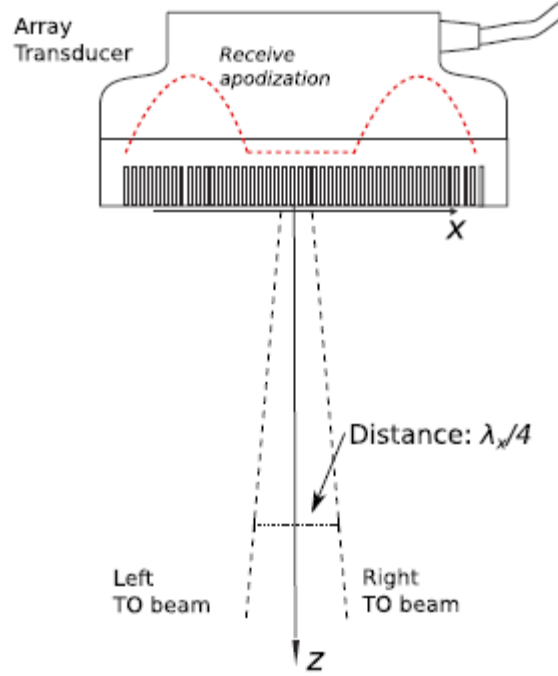


Fig. II- 14 Illustration of transverse oscillating. The apodization applied on the linear array transducer for generating left and right two beams. Reproduced with permission from [73].

In TO, a quadrature signal can be generated by focusing two parallel ultrasound beams displaced by a quarter wavelength  $\lambda_x / 4$  to have a  $\pi / 2$  phase shift between the beams [73].

The velocity components for axial and lateral directions can be estimated by using four samples [74] obtained from each transmission from the complex signals of two parallel ultrasound beams. Then get two components are obtained independently [75].

$$v_x = \frac{\lambda_x}{4\pi T_{prf}} \times \arctan \left( \frac{\Im(R_1(1))\Re(R_2(1)) + \Im(R_2(1))\Re(R_1(1))}{\Re(R_1(1))\Re(R_2(1)) - \Im(R_2(1))\Im(R_1(1))} \right) \quad (\text{II-20})$$

$$v_z = \frac{\lambda}{4\pi T_{prf}} \times \arctan \left( \frac{\Im(R_1(1))\Re(R_2(1)) - \Im(R_2(1))\Re(R_1(1))}{\Re(R_1(1))\Re(R_2(1)) + \Im(R_2(1))\Im(R_1(1))} \right) \quad (\text{II-21})$$

Here  $R_x(1)$  is the lag one complex autocorrelation. where  $\Im$  denotes the imaginary part and  $\Re$  is the real part.  $T_{\text{prf}}$  is the time between ultrasound pulses [66].

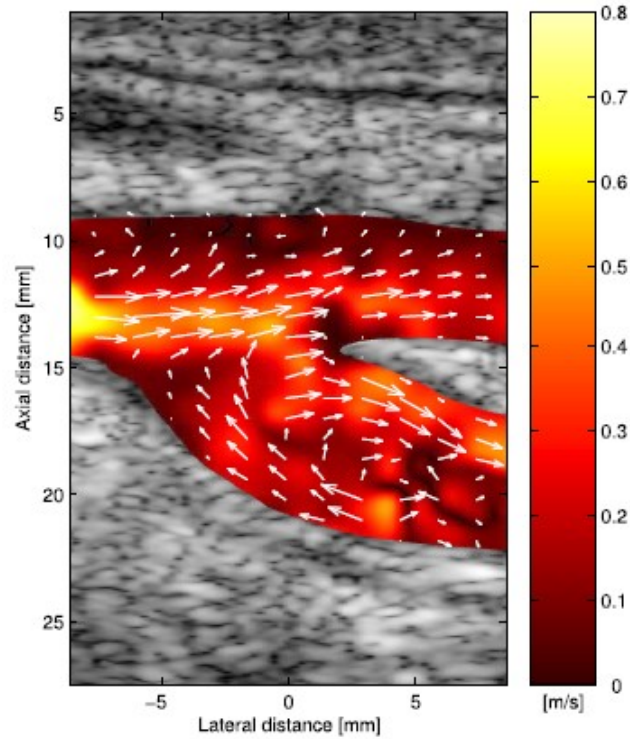


Fig. II- 15 . Transverse Oscillating vector flow image from the carotid artery. The arrows show the velocity direction, and the color shows different magnitude. Reproduced with permission from [61]

In this thesis we do not develop vector flow imaging but discuss a new pulse sequence for ultrafast imaging with improved signal-to-noise ratio that could be used to implement vector flow imaging in the future. Given that current vector flow imaging methods struggle with signal-to-noise ratio, our proposed approach should be of considerable interest.

### **III. Ultrafast Focused High-Frequency Power Doppler Imaging**

#### **A. INTRODUCTION**

Ultrafast imaging has recently demonstrated impressive capabilities for imaging blood flow in the microcirculation. Microcirculation imaging is important for assessing skin, prostate, placenta, and other organs. Imaging tumor microcirculation is essential in diagnosis and prognosis, and tracking treatment efficacy of therapeutic agents [4][24]. It is also offering unique opportunities in imaging of brain neuro-vasculature and function [40]. High-frequency ultrasound ( $>20\text{MHz}$ ) offers unique opportunities for blood flow imaging at superficial depths owing to high spatial resolution, and high backscatter from blood [26]. Most high-frequency microcirculation Power Doppler imaging methods have relied on traditional Doppler imaging sequences. Emerging ultrafast plane-wave imaging methods are further pushing the limits of sensitivity to slow flows [76]. Because depths are superficial for high-frequency ultrasound, minimal time-of-flight can also lead to high imaging rates, even with focused beam imaging [23]. In this paper we compare ultrafast focused beam imaging to traditional Power Doppler and ultrafast plane-wave methods for a 21-MHz array using a high-frequency programmable ultrasound platform.

Traditional Doppler (TD) Imaging emits multiple focused ultrasound beams along a line-of-sight and then moves to next scan-lines, repeating this process until  $M$  scanlines are acquired with an ensemble of  $N$  pulses at each scanline position. Traditional Doppler methods track scattered power of moving blood only along each respective line-of-sight.

In contrast, ultrafast ultrasound methods aim to acquire images rapidly and enable large ensemble sizes as well as enable spatio-temporal filtering which together have shown to greatly improve sensitivity to slow flow in the microcirculation.

Traditional Power Doppler methods offer focusing of the transmit energy, leading to high SNR, unlike plane-wave methods.

We investigate ultrafast high-frequency focused imaging (Data acquisition is illustrated in Fig.III-1) as compared with traditional Doppler and plane-wave imaging.

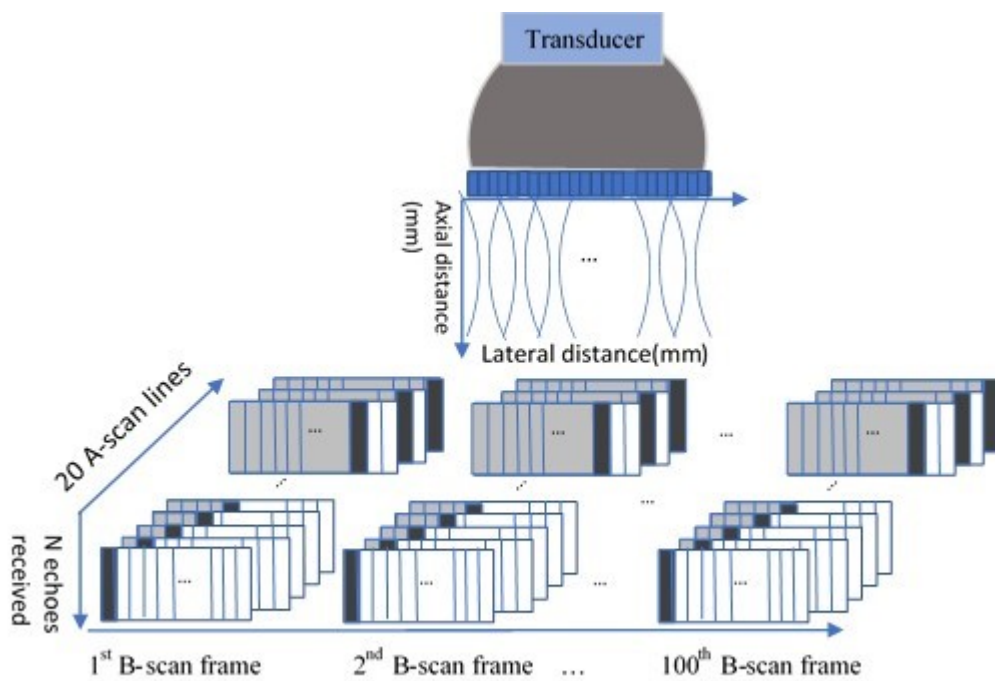


Fig. III-1 Data acquisition procedure of ultrafast high frequency focused imaging method. Each subset of transducer elements used to generate one focused ultrasound beam and using receive signal to create one A-scan until get whole B-scan frame.

High imaging rates are possible when imaging at superficial depths and a large ensemble of image frames with this approach additionally enable spatio-temporal filtering approaches, previously shown to offer advantages for flow imaging [48][34]. We use a 256-element linear array transducer with central frequency of 21MHz. We use spatiotemporal clutter filtering based on Singular-Value Decomposition (SVD) filters to remove tissue motion clutter [14]. Phantom experiments, and in vivo imaging studies are performed to compare the above-mentioned methods.

## **B. Methods**

### **1. Experimental Setup**

A Verasonics Vantage system was programmed to generate ultrasound imaging sequences. We used a high frequency linear array transducer LZ250 from FUJIFILM Visualsonics containing 256 piezoelectric elements. Table I below shows the main attributes of the transducer and parameters used during the imaging procedure.

Flow phantoms are used for comparing flow imaging methods. We use 200ml 10% concentration gelatin (G2500-1KG, SIGMA-ALDRICH) solution mixed with 50ml 10% concentration corn starch solution to mimic tissue and a ~20% corn starch solution for blood mimicking fluid [77][78]. In some experiments below we also use rat blood. We used a Polyurethane tube (PU-33-50, SAI-Infusion Technologies) with inside diameter of 0.015 inches and outside diameter of 0.033 inches. A syringe pump (NE-300, New Era Pump System, Inc.) was used to push the solution at the required flow rate. The minimum velocity achievable was 1mm/s.

TABLE 1  
PARAMETERS OF EXPERIMENT

Parameters	Value
Transducer type	VisualSonics LZ250
Transducer center frequency	21 MHz
Doppler pulse length	2 cycles
Ultrasound propagation velocity	1540 m/s
Channel data Sampling frequency	83.32 MHz
Pitch	0.16mm
Kerf	0.09mm

## 2. Comparison between imaging methods

Single-plane-wave imaging offers high-frame-rate at the cost of image quality. Multi-angle plane-wave compounding improves image quality at the cost of imaging speed [79]. We design experiments to compare all these methods. First, we used flow phantoms with a vessel located at a depth of 8mm. The transmit focal depth is defined in to be 8.5 mm.

PWI creates each B-scan through angled plane wave transmissions [63]. In comparing with single plane-wave imaging, we keep the pulse-repetition rate the same, fixed at 1KHz. To compare with multi-angle plane-wave compounding we fix the number of transmit events per image and the pulse repetition rate. In other words, we set the number of A-scan lines of UFFI to be the same as the number of angles of ultrafast compound plane wave imaging to achieve the same frame rate for both techniques. In particular, we use 32 transmits per B-scan for each of UFFI and plane-wave compounding. Again, the pulse-repetition rate is set to 1KHz.

To compare ultrafast focused imaging with traditional Doppler we keep the same PRF and the same total number of transmit events. In particular, for ultrafast focused imaging we collect 80 B-scan frames of 64 A-scan lines and for TD we collect 10 Doppler frames, each having an ensemble size of 8. In the case of the TD methods, we average the 10 Doppler frames to form one net Power Doppler image.

### **3. Impact of UFFI Ensemble Size**

To show the influence of ensemble size on the flow discrimination capability of UFFI, we designed an experiment to use UFFI to image a flow phantom with two vessels separated by less than 3 mm to get 50, 80 and 100 frames respectively. The depth of the first vessel is around 10mm and the second is 13mm.

### **4. Testing Different Flow Velocities**

To test the hypothesis that ultrafast focused scanline imaging may offer improved SNR at low flow velocities we varied flow speeds of rat blood in our phantom. Again, we set the pulse-repetition rate to 1KHz for all cases. We set the number of A-scan lines of UFFI to be the same as the number of angles of ultrafast compound plane wave imaging to achieve the same B-scan frame rate. Rat blood mixed with anticoagulant (heparin) was flowed through the phantom at speeds of 1mm/s and 1cm/s [80].

### **5. Filtering and Signal Processing**

SVD spatiotemporal filtering [48][14][45] is used to remove clutter on flow phantom images for all methods. The first 10 singular values were removed, representing tissue components. In the case of Traditional Doppler, filtering is restricted to a single A-scan line location, but we use data from all Doppler frames.

The power Doppler signal was calculated according to the beamformed IQ data:

$$PD = \left( \frac{1}{N} \sum_{n=1}^N I^2(n) + Q^2(n) \right) \quad (\text{III-22})$$

Where I is the in-phase component and Q is the Quadrature component of the signals obtained after demodulation of the RF data, and N is the ensemble size [26][81].

## 6. Experiments in vivo

A murine model was used to study our approach for blood flow imaging. We place a gas-anesthetized mouse on a pad and remove the hair on the back flank. We used the LZ250 high frequency transducer with ultrasound gel to locate the kidney of mouse. We used real time B mode ultrasound flash imaging for navigation then ran scripts to perform blood flow imaging with TD, PW and UFFI methods, respectively. The transducer attributes and imaging parameters are the same as that in Table I. All experiments were performed following protocols approved by the Animal Care and Use Committee of the University of Alberta.

A similar in vivo experiment was performed on the palm of a human subject. These were conducted using protocols approved by the University of Alberta Research Ethics Office.

## 7. Quality Metrics

To quantify signal-to-noise ratios in experimental images, we use the mean Power Doppler signal over the whole image relative to noise standard deviation acquired when imaging no object. Results are reported in dB. To quantify variance of Power Doppler signals, we manually select regions of interest where blood vessels are present and quantify the standard deviation of the Power Doppler signal, reporting the result in dB.

## C. RESULTS

### 1. Experiments with phantoms

Here we describe the results of section B.2. One angle Plane wave imaging (Flash Imaging) can acquire images very quickly but with the inevitable drawback of poor image quality, as the ultrasound beam is not transmit-focused [25]. From Fig.III-2, single-angle PWI demonstrates more noise compared to other methods and TD shows blood flow signals without continuity. Multi-angle plane wave imaging offers significantly improved performance [32], however, we can see from Fig.III-2, achieved the best image quality with lowest variance and high SNR. These images were acquired using low velocity flows ( $\sim 1\text{mm/s}$ ). The SNR of PWI, TD, ultrafast compound imaging and UFFI methods were measured to be 11.9, 21.2, 31.4 and 41.4 dB, respectively. The standard deviation in dB of PWI, TD, ultrafast compound imaging and UFFI methods were measured to be -6.1, -5.2, -7.6 and -10 dB, respectively. The area under the ROC curve as described in the methods section II.G was found to be 0.580, 0.664, 0.881, and 0.935 for PWI, TD, plane-wave compounding, and UFFI, respectively.

Fig. III-3 illustrates that when the B-scan frame-rate of UFFI is made to be the same as TD, UFFI offers greatly improved performance, both in terms of SNR and variance with the vessel. This is expected since we can achieve 160 times larger ensemble size compared with that of TD, even though the same number of transmit events is used. When the UFFI PRF is lowered to 1KHz to match that of TD, the results, shown in Fig. III-3B, are less impressive. This is also the case when the frame rate of UFFI matches the TD Doppler frame rate, but a wider image is acquired, as shown in Fig. III-3D.

Fig.III-4 shows the larger ensemble size with the proposed UFFI method, the greater the Power Doppler Sensitivity [82][42]. The SNR of 50, 80 and 100 ensemble size of UFFI methods were measured to be 30.1, 36.4 and 41.0 dB respectively. The standard deviation was measured to be -4.8, -5.3 and -6.4 dB. The area under the ROC curve was found to be 0.622, 0.794, and 0.881 for ensemble sizes of 50, 80 and 100, respectively.

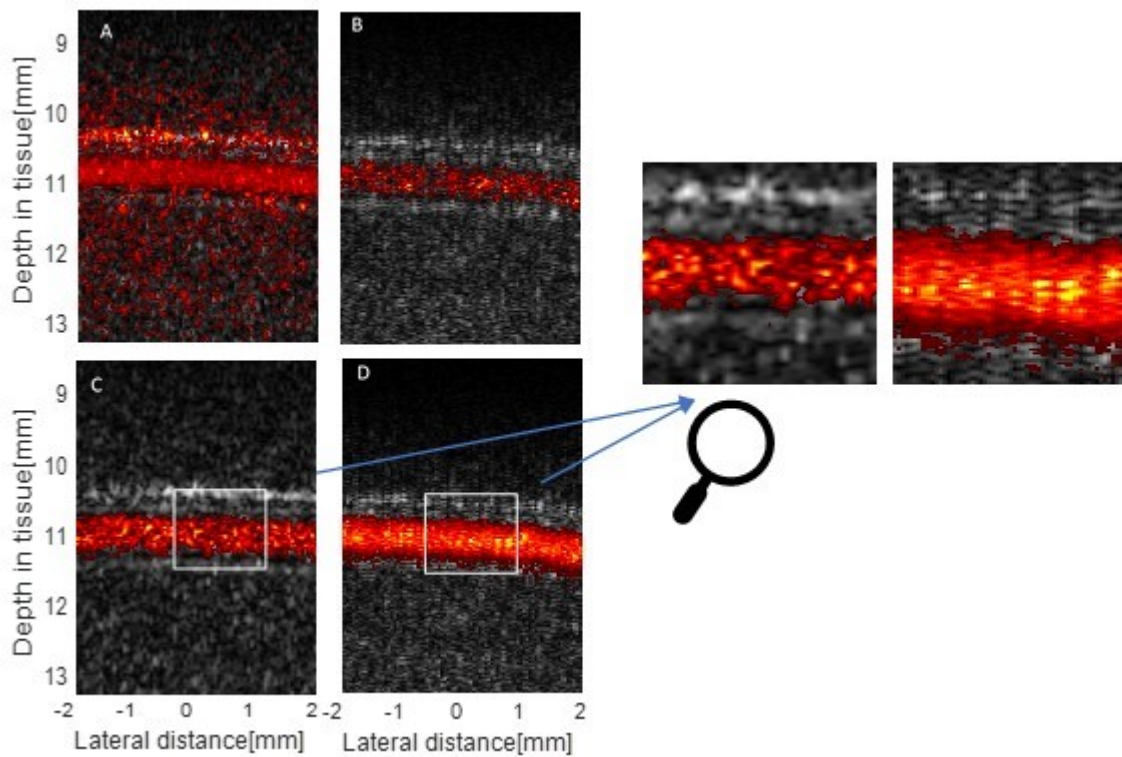


Fig. III-2 Power Doppler images of flow phantom with vessel located at 10-11 mm penetration. Flow velocity is 1mm/s. (A) Plane Wave Imaging method with prf and frame rate 1KHz; (B) Traditional Doppler method with prf 1KHz; (C) 32 angles ultrafast compounding imaging method with prf 1KHz; (D) UFFI (Fast Walking Aperture) method with 32 A-scan lines for one B-scan, prf is 1KHz.

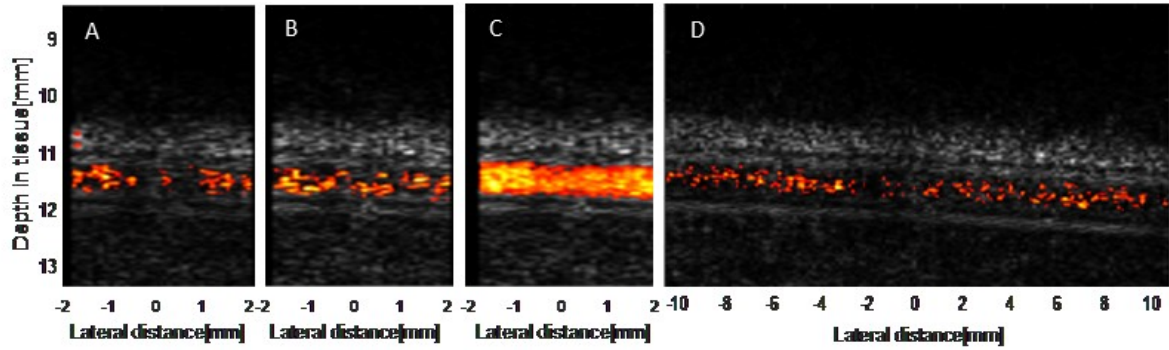


Fig. III-3. Power Doppler images of a flow phantom with mean flow velocity set to 1 cm/s using methods described in Section II.B. (A) Traditional Doppler method, the pulse repetition frequency (PRF) is 1 kHz; (B) Ultrafast Focused Imaging (UFFI), PRF is 1 kHz; (C) UFFI with frame rate set to 1 kfps, equal to the PRF of Traditional Doppler in A; (D) UFFI with the same frame rate and acquisition time and acquisition time as Traditional Doppler. In this case a larger field-of-view is acquired at the cost of Power Doppler sensitivity.

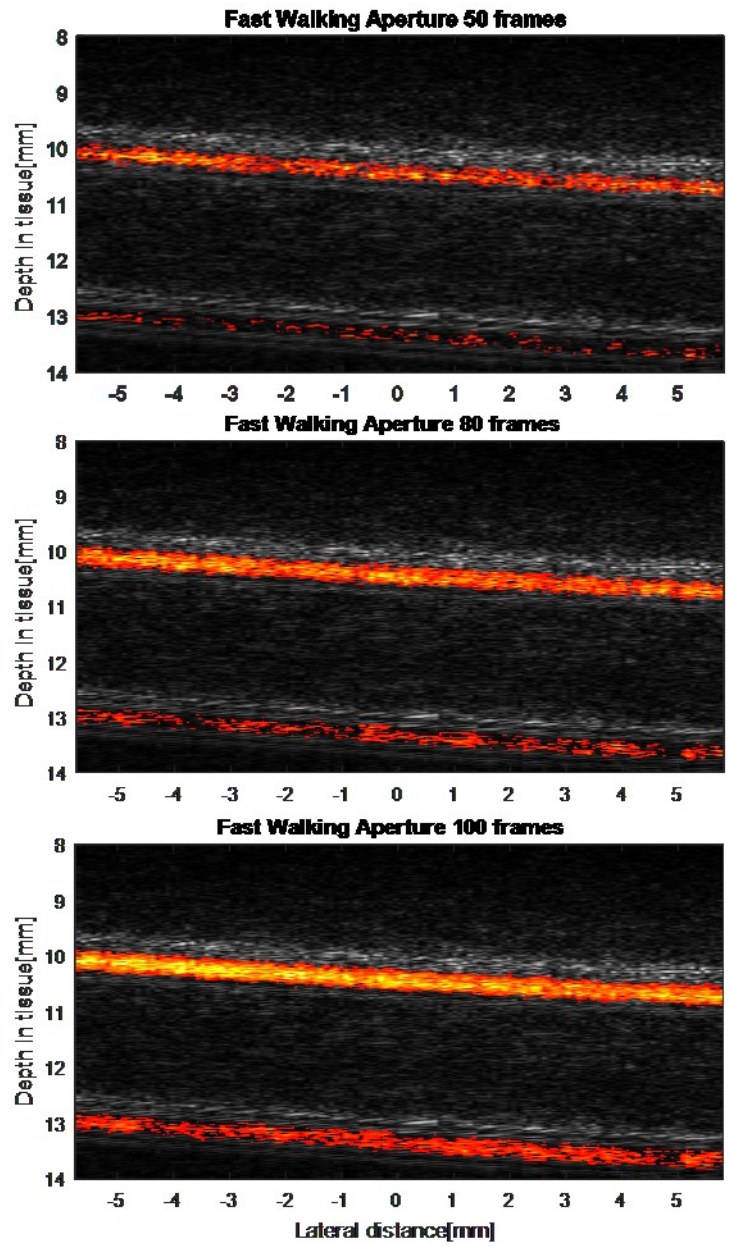


Fig. III-3 Power Doppler images of flow phantom with two vessels located at depth of 10mm and 13mm.  
 (A) UFFI with ensemble size 50; (B) UFFI with ensemble size 80; (C) UFFI with ensemble size 100.

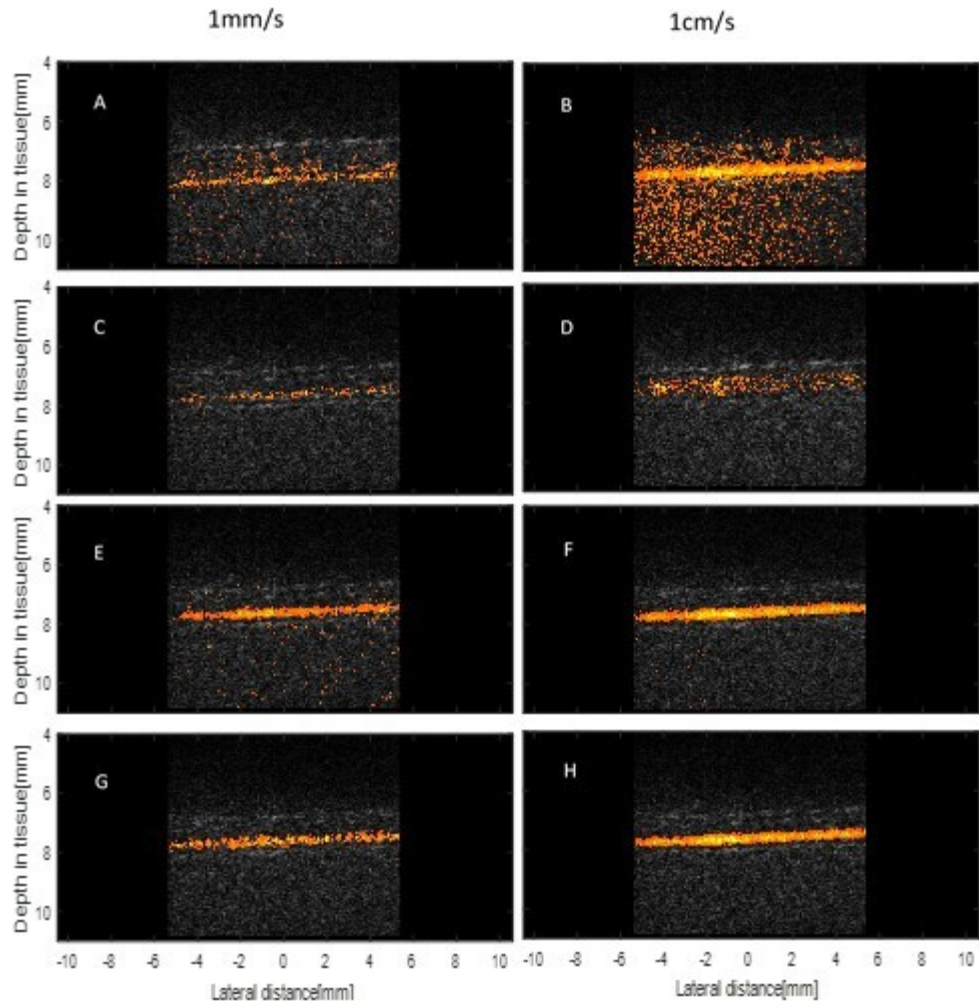


Fig. III-4 Power Doppler images of flow phantom with the vessel located at depth of 8mm. The left column is imaging blood flow of 1mm/s, the right column is for 1cm/s blood flow. We use 1KHz PRF for all cases. (A) and (B). PWI method; (C) and (D). TD method; (E) and (F). 32-angle-Plane-wave compounding method; (G) and (H). UFFI method.

Fig. III-5 demonstrates that at blood flow velocities down to 1mm/s and up to 1cm/s, UFFI provides the highest SNR and lowest variance. Single plane-wave imaging, in particular, suffers from poor SNR for both flow velocities. Traditional Doppler offers improved SNR, but the variance is poor. Plane wave compounding offers improvements, but SNR and variance are still inferior to UFFI, especially at low flow velocities. The measured SNR and standard deviation are shown in below Table II:

TABLE 2 MEASURED SNR AND STANDARD DEVIATION

	SNR(dB)		Standard Deviation (dB)		AUC	
	1mm/s	1cm/s	1mm/s	1cm/s	1mm/s	1cm/s
PWI	11.2	10.0	-4.9	-5.2	0.533	0.590
TD	18.1	22.0	-4.7	-5.2	0.538	0.621
Compounding	28.1	35.1	-6.3	-7.3	0.866	0.922
UFFI	33.3	42.3	-6.6	-7.6	0.900	0.945

## 2. In vivo study

Fig.III-6 shows the Power Doppler images of a mouse’s kidney, acquired with different methods. Fig. III-6A shows the UFFI method with measured SNR 39.2dB compared with Traditional Doppler with SNR 25.4dB (Fig.III-6B) and plane-wave Doppler with SNR 13.3dB (Fig.III-6C). The area under the ROC curve was calculated to be 0.733, 0.630 and 0.560 for PWI, TD, and UFFI, respectively.

Again, UFFI offers greater Power Doppler sensitivity and lower noise compared with the other methods. This is also seen in the image of the human palm, shown in Fig. III-7. The SNR of PWI, TD, ultrafast compound imaging and UFFI methods were measured to be 13.4, 20.3, 34.2 and 40.5

dB, respectively. The area under the ROC curve was measured to be 0.583, 0.703, 0.890, and 0.906 for PWI, TD, plane-wave compounding, and UFFI, respectively.

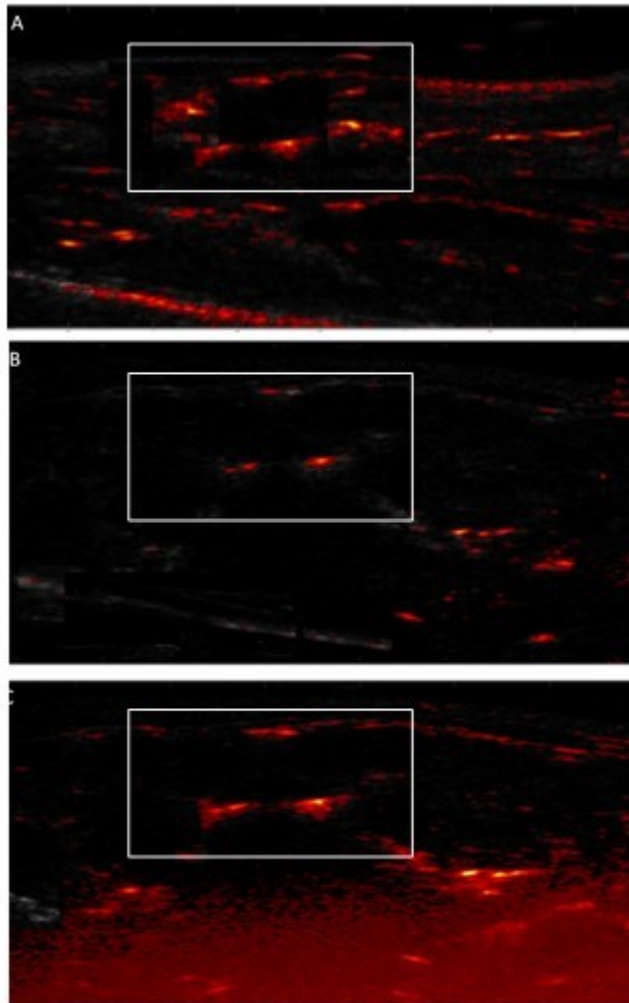


Fig. III-5 Power Doppler images of blood flow in the kidney of a mouse. (A) UFFI method; (B) Traditional Doppler imaging. (C) Single angle plane wave imaging.

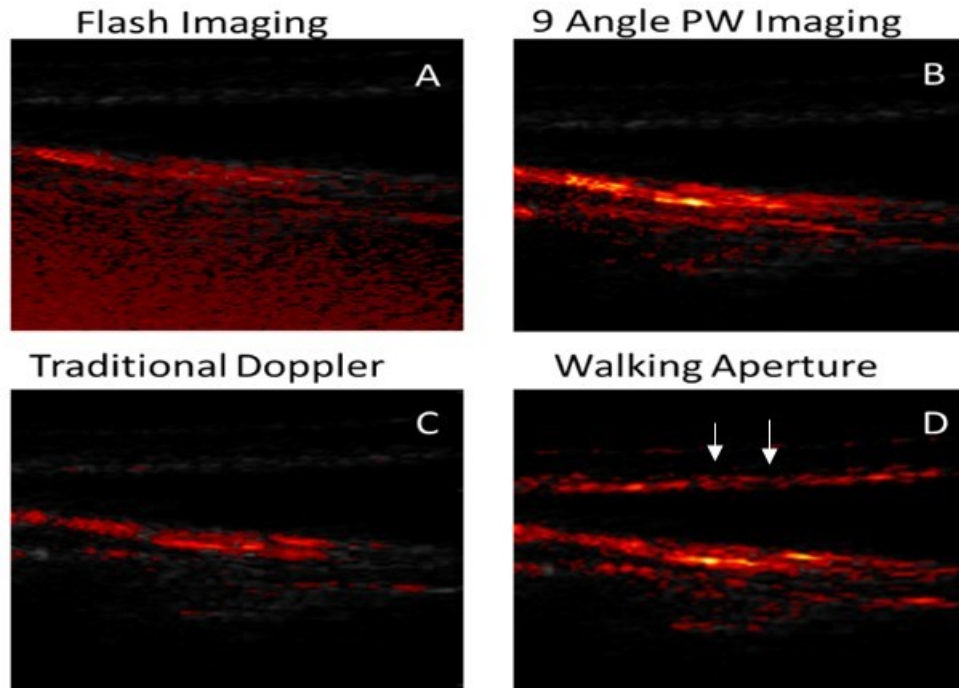


Fig. III-6 Power Doppler blood flow images of the palm of hand. (A) PW imaging with one direction. (B) 9 angles PW imaging. (C) Traditional Doppler method. (D) UFFI (fast walking aperture) imaging method

#### D. DISCUSSION

UFFI imaging is based on fast successive emissions of high frequency focused ultrasound waves. The backscattered echoes from these focused beams transmission are combined line by line, frame by frame and reconstructed to resynthesize ultrasound images which exhibit higher image quality and improved frame rate.

It should be mentioned that in all cases, we set the transmit voltage to 40V. This is the maximum voltage that the transducer could safely be operated at. If we were not limited by the transmit

voltage, and instead were limited by ultrasound safety parameters (such as the mechanical index and thermal index) it could be possible that plane-wave methods could use a higher transmit level and achieve improved SNR. However, signal variance may not necessarily be improved.

Overall, we found that UFFI methods offered high SNR due to beam focusing, and high Doppler detection performance (as quantified by the area under the ROC curves) due to fast acquisition and large ensemble sizes, compared with other techniques.

UFFI does have the limitation of requiring imaging over small window sizes, however, multiple window acquisitions can be mosaicked to form a larger image.

## **E. Conclusion**

This paper compared different approaches for blood flow imaging. Ultrafast high-frequency focused beam imaging has the potential to provide ultrafast imaging with higher SNR and lower variance than one angle plane wave imaging at the same frame rate. Also, when using ultrafast high frequency focused imaging in flow phantom experiment, we acquired images with higher SNR than those acquired at the same frame rate by multi-angle plane wave imaging. By contrast with traditional Doppler imaging, UFFI shows advantages on imaging speed, sensitivity of slow flows and width of image region. Traditional Doppler is not sensitive to slow flows due to the slow imaging speed [57]. Current work is exploring velocity estimation methods to extend current work on Power Doppler for high-frequency arrays.

## IV. Conclusion and Future work

### A. Summary of work done in this thesis

In summary, we demonstrated high-resolution sensitive blood flow imaging using high-frequency array transducers and novel pulse-sequence- and processing techniques.

We implemented both simulation and experiments to compare our proposed Ultrafast Focused Imaging (UFFI) method with Traditional Doppler Imaging, Plane Wave Imaging and Plane Wave Compounding. Since UFFI use focused ultrasound beams, compared with other ultrafast imaging methods, it demonstrates advantages including higher SNR, improved sensitivity, and lower variance than both Plane Wave Imaging and Plane Wave Compounding techniques. By contrast with Traditional Doppler Imaging, UFFI shows higher imaging speed, and improved sensitivity. Larger ensemble size and improved SNR due to focusing enable the proposed UFFI method to provide improved image quality compared to the other methods discussed, where attempts were made to make fair comparisons, including keeping some parameters fixed between comparisons. The comparison can be summarized as follows:

1. Compared with Traditional Doppler Imaging: UFFI offers improved B-scan imaging speed and Power Doppler sensitivity when keeping the same pulse repetition frequency, same Doppler frame rate and same data acquisition time
2. Compared with Plane Wave Imaging: UFFI offers improved Power Doppler sensitivity and lower variance when keeping the same ensemble size. Additionally B-scan image quality is improved.
3. Compared with Plane Wave Compounding: UFFI provides reduced variance and improved Power Doppler sensitivity when keeping the same ensemble size and the same B-scan

imaging frame-rate. Here the number of plane wave compounding angles is the same as the number of lines of Ultrafast Focused Imaging to achieve the same frame rate.

Ultrafast Focused Imaging shows higher SNR and better sensitivity on both phantom study and experiments in vivo compared with other three imaging methods, especially for slow velocity flows.

## **B. Future work**

### **1. Clinical Translation**

The current developments have been implemented with offline processing. Additional work should aim to achieve real-time implementation and clinical translation for cancer, diabetes, cardiovascular medicine, neurovascular imaging, and other applications.

### **2. Blood velocity estimation**

Current work will involve exploring velocity estimation methods to extend UFFI methods for improved Color-Flow imaging using high-frequency arrays. We are investigating Kasai autocorrelation algorithms to estimate velocity for UFFI-based blood-flow imaging. Future work could also include improved vector-flow imaging. Our hypothesis is that UFFI should enable improved velocity estimation and sensitivity to slow flows in the microcirculation.

### **3. Combining Photoacoustic Imaging and Ultrafast Focused Imaging**

The rate of oxygen metabolism is an important potential metric that could be of considerable clinical importance. The capability to accurately image the rate of oxygen consumption has been

a sought-after goal. However, current methods suffer from severe limitations and lack quantitation. Recently, our group demonstrated the combination of photoacoustic imaging and Doppler ultrasound to measure oxygen flux and metabolic rate of oxygen consumption. Multi-wavelength photoacoustic imaging is capable of estimating blood oxygen saturation. Paired with the ability of Doppler ultrasound to image blood flow, the combined techniques offer considerable potential for oxygen metabolism estimation of tissues and organs such as the brain. However, our recent work was limited to a mechanically-scanned single-element transducer. Additional work should extend contributions in this thesis to imaging blood flows in combination with photoacoustic imaging using a high-frequency array transducer. This may enable much faster image acquisitions and more accurate oxygen flux estimates.

## BIBLIOGRAPHY

- [1] D. E. Goertz, J. L. Yu, R. S. Kerbel, P. N. Burns, and F. S. Foster, “High-Frequency Doppler Ultrasound Monitors the Effects of Antivascular Therapy on Tumor Blood Flow Advances in Brief High-Frequency Doppler Ultrasound Monitors the Effects of Antivascular Therapy on Tumor Blood Flow,” pp. 6371–6375, 2002.
- [2] D. Christopher, P. Burns, B. G. Starkoski, and F. S. Foster, “A high-frequency pulsed-wave Doppler ultrasound system for the detection and imaging of blood flow in the microcirculation,” *Ultrasound Med. Biol.*, vol. 23, no. 7, pp. 997–1015, 1997.
- [3] D. A. Christopher, P. N. Burns, J. Armstrong, and F. S. Foster, “A High-Frequency Continuous-Wave Doppler Ultrasound System for the Detection of Blood Flow in the Microcirculation,” *Ultrasound Med. Biol.*, vol. 22, no. 9, pp. 1191–1203, 1996.
- [4] B. R. Zetter, “Angiogenesis and Tumor,” no. 1, 1998.
- [5] B. D. de Senneville *et al.*, “Development of a fluid dynamic model for quantitative contrast-enhanced ultrasound imaging,” *IEEE Trans. Med. Imaging*, vol. 11, no. APRIL, 2017.
- [6] F. Stuart Foster, P. N. Burns, D. H. Simpson, S. R. Wilson, D. A. Christopher, and D. E. Goertz, “Ultrasound for the visualization and quantification of tumor microcirculation,” *Cancer Metastasis Rev.*, vol. 19, no. 1–2, pp. 131–138, 2000.
- [7] P. Carmeliet and M. Baes, “clinical implications of basic research Metabolism and Therapeutic Angiogenesis,” *Society*, pp. 2511–2512, 2008.
- [8] D. E. Goertz, D. A. Christopher, J. L. Yu, R. S. Kerbel, P. N. Burns, and F. S. Foster, “High-frequency color flow imaging of the microcirculation,” *Ultrasound Med. Biol.*, vol. 26, no. 1, pp. 63–71, 2000.
- [9] N. G. Pandian *et al.*, “Ultrasound Angioscopy: Real-Time, Two-Dimensional, Intraluminal Ultrasound Imaging of Blood Vessels,” *Am. J. Cardiol.*, vol. 62, no. mm, pp. 493–494, 1988.

- [10] M. P. Hartung, T. M. Grist, and C. J. François, “Magnetic resonance angiography: Current status and future directions,” *J. Cardiovasc. Magn. Reson.*, vol. 13, no. 1, pp. 1–11, 2011.
- [11] A. F. Kopp *et al.*, “Non-invasive coronary angiography with high resolution multidetector-row computed tomography: Results in 102 patients,” *Eur. Heart J.*, vol. 23, no. 21, pp. 1714–1725, 2002.
- [12] S. Valable *et al.*, “Complementary information from magnetic resonance imaging and  $^{18}\text{F}$ -fluoromisonidazole positron emission tomography in the assessment of the response to an antiangiogenic treatment in a rat brain tumor model,” *Nucl. Med. Biol.*, vol. 38, no. 6, pp. 781–793, 2011.
- [13] P. Song *et al.*, “Accelerated Singular Value-Based Ultrasound Blood Flow Clutter Filtering with Randomized Singular Value Decomposition and Randomized Spatial Downsampling,” *IEEE Trans. Ultrason. Ferroelectr. Freq. Control*, vol. 64, no. 4, pp. 706–716, 2017.
- [14] F. W. Mauldin, D. Lin, and J. A. Hossack, “The singular value filter: A general filter design strategy for pca-based signal separation in medical ultrasound imaging,” *IEEE Trans. Med. Imaging*, vol. 30, no. 11, pp. 1951–1954, 2011.
- [15] Wagner FC1, Macovski A, Nishimura DG. “Dual-energy x-ray projection imaging: two sampling schemes for the correction of scattered radiation” *Med Phys.* Sep-Oct;15(5):732-48, 1988.
- [16] Jiang Hsieh, *Computed Tomography: Principles, Design, Artifacts, and Recent Advances, Third Edition.* .
- [17] K. K. Kwong *et al.*, “Dynamic magnetic resonance imaging of human brain activity during primary sensory stimulation.,” *Proc. Natl. Acad. Sci. U. S. A.*, vol. 89, no. 12, pp. 5675–5679, 1992.
- [18] T. A. Holly *et al.*, “Single photon-emission computed tomography,” *J. Nucl. Cardiol.*, vol. 17, no. 5, pp. 941–973, 2010.
- [19] P. E. V. and M. N. M. (Eds) Dale L Bailey, David W Townsend, *Positron Emission Tomography.* 2005.

- [20] P. Beard, "Biomedical photoacoustic imaging," *Interface Focus*, vol. 1, no. 4, pp. 602–631, 2011.
- [21] A. G. Bell, "On the production and reproduction of sound by light," *Am. J. Sci.*, vol. s3-20, no. 118, pp. 305–324, 1880.
- [22] J. a. Jensen, "Simulation of advanced ultrasound systems using Field II," *2004 2nd IEEE Int. Symp. Biomed. Imaging Nano to Macro (IEEE Cat No. 04EX821)*, pp. 636–639, 2004.
- [23] M. Tanter and M. Fink, "Ultrafast imaging in biomedical ultrasound," *IEEE Trans. Ultrason. Ferroelectr. Freq. Control*, vol. 61, no. 1, pp. 102–119, 2014.
- [24] S. Arslan, A. Y. Karahan, F. Oncu, S. Bakdik, M. S. Durmaz, and I. Tolu, "Diagnostic Performance of Superb Microvascular Imaging and Other Sonographic Modalities in the Assessment of Lateral Epicondylitis," *J. Ultrasound Med.*, 2017.
- [25] H. Patriquin, M. Lafortune, D. S. Babcock, H. Patriquin, M. Lafortune, and M. Dauzat, "Power Doppler sonography : basic principles and clinical applications in children," *Pediatr. Radiol.*, vol. 26, no. 2, pp. 109–115, 1996.
- [26] X. Xu, L. Sun, J. M. Cannata, J. T. Yen, and K. K. Shung, "High-frequency ultrasound Doppler system for biomedical applications with a 30-MHz linear array.," *Ultrasound Med. Biol.*, vol. 34, no. 4, pp. 638–46, 2008.
- [27] J. Yang, C. Pang, X.-D. Song, and X. Gao, "A Method for Gray-Scale Imaging of Blood Flow Using High-Frequency Ultrasound," *Ultrason. Imaging*, vol. 40, no. 1, pp. 3–14, 2018.
- [28] J. E. Kennedy, G. R. Ter Haar, and D. Cranston, "High intensity focused ultrasound: surgery of the future?," *Br. J. Radiol.*, vol. 76, no. 909, pp. 590–599, 2003.
- [29] A. Swillens, L. Lovstakken, J. Kips, H. Torp, and P. Segers, "Ultrasound simulation of complex flow velocity fields based on computational fluid dynamics," *IEEE Trans Ultrason Ferroelectr Freq Control*, vol. 56, no. 3, pp. 546–556, 2009.
- [30] S. Fadnes, I. K. Ekroll, S. A. Nytnes, H. Torp, and L. Lovstakken, "Robust angle-independent blood velocity estimation based on multi-angle speckle tracking and vector Doppler," *IEEE Int. Ultrason. Symp. IUS*, pp. 337–340, 2014.

- [31] M. Cikes, L. Tong, G. R. Sutherland, and J. D’Hooge, “Ultrafast cardiac ultrasound imaging: Technical principles, applications, and clinical benefits,” *JACC Cardiovasc. Imaging*, vol. 7, no. 8, pp. 812–823, 2014.
- [32] E. Tiran *et al.*, “Multiplane wave imaging increases signal-to-noise ratio in ultrafast ultrasound imaging,” *Phys. Med. Biol.*, vol. 60, no. 21, pp. 8549–8566, 2015.
- [33] T. Reichl, J. Passenger, O. Acosta, and O. Salvado, “Ultrasound goes GPU: real-time simulation using CUDA,” vol. 726116, no. March 2009, p. 726116, 2009.
- [34] P. Song, A. Manduca, J. D. Trzasko, and S. Chen, “Noise Equalization for Ultrafast Plane Wave Microvessel Imaging,” *IEEE Trans. Ultrason. Ferroelectr. Freq. Control*, vol. 64, no. 11, pp. 1776–1781, 2017.
- [35] G. Montaldo, M. Tanter, J. Bercoff, N. Benech, and M. Fink, “Coherent plane-wave compounding for very high frame rate ultrasonography and transient elastography,” *IEEE Trans. Ultrason. Ferroelectr. Freq. Control*, vol. 56, no. 3, pp. 489–506, 2009.
- [36] J. Bercoff *et al.*, “Ultrafast compound doppler imaging: Providing full blood flow characterization,” *IEEE Trans. Ultrason. Ferroelectr. Freq. Control*, vol. 58, no. 1, pp. 134–147, 2011.
- [37] T. Harrison and R. J. Zemp, “The applicability of ultrasound dynamic receive beamformers to photoacoustic imaging,” *IEEE Trans. Ultrason. Ferroelectr. Freq. Control*, vol. 58, no. 10, pp. 2259–2263, 2011.
- [38] Z. Li and C. Chi, “Fast computation of far-field pulse-echo PSF of arbitrary arrays for large sparse 2-D ultrasound array design,” *Ultrasonics*, vol. 84, pp. 63–73, 2018.
- [39] A. E. C. M. Saris, H. H. G. Hansen, S. Fekkes, M. M. Nillesen, M. C. M. Rutten, and C. L. De Korte, “A Comparison Between Compounding Techniques Using Large Beam-Steered Plane Wave Imaging for Blood Vector Velocity Imaging in a Carotid Artery Model,” *IEEE Trans. Ultrason. Ferroelectr. Freq. Control*, vol. 63, no. 11, pp. 1758–1771, 2016.
- [40] E. MacÉ, G. Montaldo, I. Cohen, M. Baulac, M. Fink, and M. Tanter, “Functional ultrasound

- imaging of the brain,” *Nat. Methods*, vol. 8, no. 8, pp. 662–664, 2011.
- [41] C. Kasai, K. Namekawa, A. Koyano, and R. Omoto, “Real-Time Two-Dimensional Blood Flow Imaging Using an Autocorrelation Technique,” *IEEE Trans. Sonics Ultrason.*, vol. 32, no. 3, pp. 458–464, 1985.
- [42] T. Loupas, R. W. Gill, and J. T. Powers, “An Axial Velocity Estimator for Ultrasound Blood Flow Imaging, Based on a Full Evaluation of the Doppler Equation by Means of a Two-Dimensional Autocorrelation Approach,” *IEEE Trans. Ultrason. Ferroelectr. Freq. Control*, vol. 42, no. 4, pp. 672–688, 1995.
- [43] B.-F. Osmanski, M. Pernot, G. Montaldo, A. Bel, E. Messas, and M. Tanter, “Ultrafast Doppler imaging of blood flow dynamics in the myocardium,” *IEEE Trans. Med. Imaging*, vol. 31, no. 8, pp. 1661–8, 2012.
- [44] M. Lenge, A. Ramalli, P. Tortoli, C. Cachard, and H. Liebgott, “Plane-wave Transverse Oscillation for High Frame Rate 2-D Vector Flow Imaging,” *IEEE Trans. Ultrason. Ferroelectr. Freq. Control*, vol. 62, no. 12, pp. 2126–2137, 2015.
- [45] P. Song, A. Manduca, J. D. Trzasko, and S. Chen, “Ultrasound small vessel imaging with block-wise adaptive local clutter filtering,” *IEEE Trans. Med. Imaging*, vol. 36, no. 1, pp. 251–262, 2017.
- [46] S. W. Smith, H. G. P. Jr, O. T. Von Ramm, U. S. Food, D. Adm, and M. D. Rockville, “High-speed ultrasound volumetric imaging system. I. Transducerdesign and beam steering,” *IEEE Trans. Ultrason. Ferroelectr. Freq. Control*, vol. 38, no. 2, pp. 100–108, 1991.
- [47] G. R. Lockwood, D. H. Turnbull, D. A. Christopher, and F. S. Foster, “Beyond 30 MHz - applications of high-frequency ultrasound imaging,” *IEEE Eng. Med. Biol. Mag.*, vol. 15, pp. 60–71, 1996.
- [48] C. Demené *et al.*, “Spatiotemporal Clutter Filtering of Ultrafast Ultrasound Data Highly Increases Doppler and fUltrasound Sensitivity,” *IEEE Trans. Med. Imaging*, vol. 34, no. 11, pp. 2271–2285, 2015.

- [49] A. J. Y. Chee, B. Y. S. Yiu, and A. C. H. Yu, "A GPU-Parallelized Eigen-Based Clutter Filter Framework for Ultrasound Color Flow Imaging," *IEEE Trans. Ultrason. Ferroelectr. Freq. Control*, vol. 64, no. 1, pp. 150–163, 2017.
- [50] W. You and Y. Wang, "A fast algorithm for adaptive clutter rejection in ultrasound color flow imaging based on the first-order perturbation: A simulation study," *IEEE Trans. Ultrason. Ferroelectr. Freq. Control*, vol. 57, no. 8, pp. 1884–1889, 2010.
- [51] D. E. Kruse and K. W. Ferrara, "A new high resolution colour flow system using an eigendecomposition-based adaptive filter for clutter rejection," *IEEE Trans. Ultrason. Ferroelec., Freq. Contr.*, vol. 49, no. 1, pp. 1739–1754, 2002.
- [52] S. Bjærum, H. Torp, and K. Kristoffersen, "Clutter filters adapted to tissue motion in ultrasound color flow imaging," *IEEE Trans. Ultrason. Ferroelectr. Freq. Control*, vol. 49, no. 6, pp. 693–704, 2002.
- [53] D. Muti and S. Bourennane, "Multidimensional filtering based on a tensor approach," *Signal Processing*, vol. 85, no. 12, pp. 2338–2353, 2005.
- [54] L. De Lathauwer, B. De Moor, Vandewalle, and J. Vandewalle, "A multilinear singular value decomposition," *SIAM J. Matrix Anal. Appl.*, vol. 21, no. 4, pp. 1253–1278, 2000.
- [55] A. C. H. Yu and L. Lovstakken, "Eigen-based clutter filter design for ultrasound color flow imaging: A review," *IEEE Trans. Ultrason. Ferroelectr. Freq. Control*, vol. 57, no. 5, pp. 1096–1111, 2010.
- [56] L. D. E. Lathauwer, B. D. E. Moor, and J. Vandewalle, "On the best rank-1 and rank- $r$ ," vol. 21, no. 4, pp. 1324–1342, 2000.
- [57] M. Kim, C. K. Abbey, J. Hedhli, L. W. Dobrucki, and M. F. Insana, "Expanding Acquisition and Clutter Filter Dimensions for Improved Perfusion Sensitivity," *IEEE Trans. Ultrason. Ferroelectr. Freq. Control*, vol. 64, no. 10, pp. 1429–1438, 2017.
- [58] A. Swillens, P. Segers, H. Torp, and L. Løvstakken, "Two-dimensional blood velocity estimation with ultrasound: Speckle tracking versus crossed-beam vector doppler based on flow simulations

- in a carotid bifurcation model,” *IEEE Trans. Ultrason. Ferroelectr. Freq. Control*, vol. 57, no. 2, pp. 327–339, 2010.
- [59] V. Sboros and M. X. Tang, “The assessment of microvascular flow and tissue perfusion using ultrasound imaging,” *Proc. Inst. Mech. Eng. Part H J. Eng. Med.*, vol. 224, no. 2, pp. 273–290, 2010.
- [60] J. Jensen, S. Nikolov, A. C. H. Yu, and D. Garcia, “Ultrasound Vector Flow Imaging: I: Sequential Systems,” *IEEE Trans. Ultrason. Ferroelectr. Freq. Control*, vol. 63, no. 11, pp. 1704–1721, 2016.
- [61] N. Oddershede and J. A. Jensen, “Effects influencing focusing in synthetic aperture vector flow imaging,” *IEEE Trans. Ultrason. Ferroelectr. Freq. Control*, vol. 54, no. 9, pp. 1811–1825, 2007.
- [62] S. Dort, S. Muth, A. Swillens, P. Segers, G. Cloutier, and D. Garcia, “Vector Flow Mapping Using Plane Wave Ultrasound Imaging,” pp. 330–333, 2012.
- [63] J. Flynn, R. Daigle, L. Pflugrath, and P. Kaczkowski, “High framerate vector velocity blood flow imaging using a single planewave transmission angle,” *IEEE Int. Ultrason. Symp. IUS*, pp. 323–325, 2012.
- [64] C. Xu and L. Prince, “Gradient Vector Flow Deformable Models,” *Handb. Med. Image*, vol. 64, no. September, pp. 9–18, 2000.
- [65] N. Paragios and O. M. Visvanathan, “Gradient Vector Flow Fast Geodesic Active Contours,” vol. 26, no. 3, pp. 402–407, 1987.
- [66] J. Flynn, R. Daigle, L. Pflugrath, K. Linkhart, and P. Kaczkowski, “Estimation and display for vector Doppler imaging using planewave transmissions,” *IEEE Int. Ultrason. Symp. IUS*, pp. 413–418, 2011.
- [67] J. Udesen, F. Gran, K. L. Hansen, J. A. Jensen, C. Thomsen, and M. B. Nielsen, “High frame-rate blood vector velocity imaging using plane waves: Simulations and preliminary experiments,” *IEEE Trans. Ultrason. Ferroelectr. Freq. Control*, vol. 55, no. 8, pp. 1729–1743, 2008.
- [68] F. Gran, J. Udesen, M. B. Nielsen, and J. A. Jensen, “Coded ultrasound for blood flow estimation

- using subband processing,” *IEEE Trans. Ultrason. Ferroelectr. Freq. Control*, vol. 55, no. 10, pp. 2211–2220, 2008.
- [69] J. A. Ketterling *et al.*, “High-speed, high-frequency ultrasound, in utero vector-flow imaging of mouse embryos,” *Sci. Rep.*, vol. 7, no. 1, pp. 1–9, 2017.
- [70] K. Gijsbertse, A. Sprengers, H. Naghibi Beidokhti, M. Nillesen, C. de Korte, and N. Verdonchot, “Strain imaging of the lateral collateral ligament using high frequency and conventional ultrasound imaging: an ex-vivo comparison,” *J. Biomech.*, 2018.
- [71] M. Anderson, “Spatial quadrature: a novel technique for multi-dimensional velocity estimation,” *1997 IEEE Ultrason. Symp. Proceedings. An Int. Symp. (Cat. No.97CH36118)*, vol. 2, pp. 1233–1238, 1997.
- [72] J. Jensen, S. Nikolov, A. C. H. Yu, and D. Garcia, “Ultrasound Vector Flow Imaging: II: Parallel Systems,” *IEEE Trans. Ultrason. Ferroelectr. Freq. Control*, vol. 3010, no. c, pp. 1–1, 2016.
- [73] J. A. Jensen, A. H. Brandt, and M. B. Nielsen, “Convex array vector velocity imaging using transverse oscillation and its optimization,” *IEEE Trans. Ultrason. Ferroelectr. Freq. Control*, vol. 62, no. 12, pp. 2043–2053, 2015.
- [74] N. Ray and S. T. Acton, “Motion gradient vector flow: An external force for tracking rolling leukocytes with shape and size constrained active contours,” *IEEE Trans. Med. Imaging*, vol. 23, no. 12, pp. 1466–1478, 2004.
- [75] K. L. Hansen *et al.*, “Vector Flow Imaging Compared with Conventional Doppler Ultrasound and Thermodilution for Estimation of Blood Flow in the Ascending Aorta,” *Ultrason. Imaging*, vol. 39, no. 1, pp. 3–18, 2017.
- [76] O. D. Kripfgans, J. M. Rubin, A. L. Hall, and J. B. Fowlkes, “Vector Doppler imaging of a spinning disc ultrasound Doppler phantom,” *Ultrasound Med. Biol.*, vol. 32, no. 7, pp. 1037–1046, 2006.
- [77] K. V. Ramnarine, D. K. Nassiri, P. R. Hoskins, and J. Lubbers, “Validation of a new blood-mimicking fluid for use in Doppler flow test objects,” *Ultrasound Med. Biol.*, vol. 24, no. 3, pp.

- 451–459, 1998.
- [78] P. R. Hoskins, “Simulation and Validation of Arterial Ultrasound Imaging and Blood Flow,” *Ultrasound Med. Biol.*, vol. 34, no. 5, pp. 693–717, 2008.
- [79] J. B. L. S. Mickael Tanter and M. Fink, “Ultrafast Compound Imaging for 2-D Motion Vector Estimation: Application to Transient Elastography,” vol. 49, no. 10, pp. 1–12, 2002.
- [80] C. N. Berry, D. Girard, S. Lochot, and C. Lecoffre, “Antithrombotic actions of argatroban in rat models of venous, ‘mixed’ and arterial thrombosis, and its effects on the tail transection bleeding time,” *Br. J. Pharmacol.*, vol. 113, no. 4, pp. 1209–1214, 1994.
- [81] R. Lyons, “Quadrature Signals : Complex , But Not Complicated,” *Dspguru.Com*, no. November, p. 19, 2008.
- [82] T. Loupas, R. W. Gill, and R. B. Peterson, “Experimental Evaluation of Velocity and Power Estimation for Ultrasound Blood Flow Imaging, by Means of a Two-Dimensional Autocorrelation Approach,” *IEEE Trans. Ultrason. Ferroelectr. Freq. Control*, vol. 42, no. 4, pp. 689–699, 1995.